Adolescent thalamic inhibition leads to long-lasting impairments in prefrontal cortex function

Laura Benoit
Columbia University https://orcid.org/0000-0002-3735-027X
Emma Holt
Columbia University https://orcid.org/0000-0002-8086-4196
Lorenzo Posani
Columbia University
Stefano Fusi
Columbia University https://orcid.org/0000-0002-3035-6652
Alexander Harris
Columbia University https://orcid.org/0000-0001-9089-0366
Sarah Canetta
Columbia University Medical Center https://orcid.org/0000-0002-3860-2504
Christoph Kellendonk (ck491@columbia.edu)
Columbia University

Article

Keywords: schizophrenia, adolescent thalamic inhibition, prefrontal cortex

Posted Date: August 9th, 2021

DOI: https://doi.org/10.21203/rs.3.rs-730508/v1

Abstract

Impaired cortical maturation is a postulated mechanism in the etiology of neurodevelopmental disorders, including schizophrenia. In sensory cortex, activity relayed by the thalamus during a postnatal sensitive period is essential for proper cortical maturation. Whether thalamic activity also shapes prefrontal cortical maturation is unknown. Here, we show that inhibiting the midline thalamus during adolescence leads to a long-lasting decrease in thalamo-prefrontal projection density and cortical excitation. Adolescent thalamic inhibition also causes prefrontal-dependent cognitive deficits during adulthood that are associated with disrupted prefrontal cross-correlations and task outcome encoding. In contrast, thalamic inhibition during adulthood has no long-lasting consequences. Strikingly, exciting the thalamus in adulthood during a cognitive task rescues prefrontal cross-correlations, task outcome encoding, and cognitive deficits. These data point to adolescence as a sensitive window of thalamo-cortical circuit maturation. Furthermore, by supporting prefrontal network activity, boosting thalamic activity provides a potential therapeutic strategy for rescuing cognitive deficits in neurodevelopmental disorders.

Introduction

Sensitive periods denote developmental time windows of heightened plasticity during which alterations in experience can lead to long-lasting changes in the anatomy and function of the nervous system[1,2]. Frequently, these windows represent periods in which the refinement of brain circuitry and function is particularly susceptible to changes in neuronal activity. A classic example is in the visual system, where transient developmental monocular deprivation can permanently impair acuity in the deprived eye[3]. This impairment in function persists even after the deprivation in visual input is reversed, as the thalamo-cortical inputs representing the closed eye are permanently disrupted in an activity-dependent manner. While sensitive periods in the circuit refinement of sensory cortices have been well-documented[3–6], recent evidence suggests that similar transient changes in activity during postnatal development can have lasting changes in the prefrontal cortex (PFC), an associative cortical area that supports higher cognitive functioning[7–10].

Disturbances in PFC function are believed to underlie the cognitive symptoms found in psychiatric disorders, such as schizophrenia. Schizophrenia is thought to have a developmental origin[11–13], and one prominent hypothesis is that during adolescence, a vulnerable period for the development of this disorder, the maturation of the PFC is disrupted[14]. In schizophrenia, recent studies have identified a decreased correlation between activity in the thalamus and the dorsolateral PFC under resting conditions, a finding which may have a structural basis[15–17]. This decreased correlation has also been measured in patients during cognitive testing[18–21], where it has been linked to impairments in functioning. Strikingly, decreased thalamo-prefrontal connectivity was also seen in younger adolescents at high risk for psychosis, and it predicted later illness conversion[15,22,23], raising the intriguing possibility that decreased input from the thalamus could be part of the developmental etiology of PFC dysfunction in the disorder[22–25].

Here, we directly test the hypothesis that input activity from the thalamus during adolescence is important for PFC circuit maturation and that decreasing this input during adolescence will lead to long-lasting impairments in the functioning of the PFC. To address this question, we used a combination of viral genetics and the designer receptor, hM4DGi, to selectively reduce activity of the thalamus during adolescence. Using a Cre/LoxP strategy, hM4DGi expression was restricted to the midline thalamus including the medio-dorsal thalamus, an area that projects to the medial PFC (mPFC) in the mouse. We found that transient thalamic inhibition during adolescence led to several persistent changes in adulthood, including (1) deficits in two mPFC-dependent cognitive tasks, (2) decreased excitation of mPFC pyramidal cells, (3) decreased anatomical thalamo-mPFC input, (4) reduced mPFC neuron cross-correlations, and (5) impaired mPFC neuron encoding of extra-dimensional set shifting task outcomes. In contrast, inhibiting the thalamus for a comparable period during adulthood had no long-lasting effects on excitatory inputs to mPFC cells or behavior. These data point to adolescence as a sensitive time window of thalamo-cortical circuit maturation. Strikingly, enhancing thalamic excitability during adulthood rescued the behavioral deficits and restored the ability of mPFC neurons to encode task outcome in mice that received adolescent thalamic inhibition. Prior studies have suggested that the thalamic inputs act as a non-specific amplifier supporting prefrontal activity during the delay periods of working memory[26–32]. Our data suggest that the thalamus plays a broader function in facilitating mPFC activity that is not restricted to delay-response tasks. Thus, this study demonstrates first the importance of thalamic input activity during adolescence for adult prefrontal cortical circuit function and second offers therapeutic insights into how to reverse cognitive deficits arising from a developmentally altered brain.

Results

A chemogenetic approach to transiently and chronically reduce thalamic cell activity during development or adulthood

We first aimed to establish that we can inhibit thalamic activity during adolescence and adulthood. Therefore, we stereotactically injected an adeno-associated virus (AAV) carrying a Cre-dependent version of the inhibitory designer receptor, hM4DGi (hereafter referred to as hM4D), into the midline thalamus of GBX2-CreERT mice (supplemental Fig. 1a). Viral injections were performed at postnatal day P13 and Cre-mediated recombination was induced by tamoxifen injection at P15-16, at a time when GBX2 expression is restricted to the midline thalamus, thereby limiting viral spread (supplemental Fig. 1b). To determine the efficacy of hM4D-mediated inhibition of thalamic neurons, we performed whole-cell patch clamp recordings from thalamic neurons in both adolescent and adult brain slices. Application of the DREADD ligand, clozapine-n-oxide (CNO), led to a hyperpolarization of thalamic neurons consistent with activation of G-protein coupled inward rectifying potassium (GIRK) channels (supplemental Fig. 1c). Thalamic neurons in control animals did not respond to CNO. CNO-application led to comparable effects sizes in adolescent and adult brain slices that were consistent with published results in adult thalamic neurons[33]. Crucially, CNO-application hyperpolarized thalamic neurons in animals that had been exposed to twice daily intraperitoneal (i.p.) CNO injections for two weeks, suggesting that chronic CNO treatment does not

lead to hM4D receptor de-sensitization (supplemental Fig. 1c; n=15 P35 & P105 Control cells, n=13 P35 hM4D naïve cells, n=8 P35 hM4D CNO-exposed cells, n=5 P105 hM4D naïve cells, n=5 P105 hM4D CNO-exposed cells; 1-way ANOVA, effect of treatment $F(4, 41)=3.203$, $p=0.0223$; Holm-Sidak post-hoc, P35 hM4D naïve vs. Control *p=0.0480, P35 hM4D CNO-exposed vs. Control *p=0.0480, P105 hM4D naïve vs. Control *p=0.0480, P105 hM4D CNO-exposed vs. Control *p=0.0366). These data indicate that repeated hM4D activation can continuously inhibit thalamic neuron activity during adolescence and adulthood.

Adolescent but not adult thalamic inhibition leads to long lasting impairments in cognition

We then tested the long-term effects of transient thalamic inhibition during adolescence (P20-50) on prefrontal-dependent cognitive task performance. To this end, CNO (1 mg/kg) was injected twice daily in hM4D and control GFP mice from days P20-50, and the animals were tested forty days later, at P90 (Fig. 1a). To assess cognition during adulthood, we chose an operant-based Non-Match to Sample (NMS) working memory task (Fig. 1b), whose acquisition is delayed after a lesion of the mPFC[34] and an odor- and texture- based attentional set shifting task (ASST), in which the extra-dimensional set shifting component of the task (EDSS) is sensitive to mPFC lesions (Fig. 1c)[35,36]. Following adolescent thalamic inhibition from P20-50, we found that the acquisition of the NMS task was impaired in animals expressing hM4D compared with controls (Fig. 1d; n=17 Control animals, n=21 hM4D animals; learning curve: 2-way repeated measures (rm) ANOVA, effect of time $F(4.201,151.2)=102.0$, $p<0.0001$, effect of group $F(1,36)=3.143$, $p=0.0847$, effect of group x time $F(13,468)=2.088$, *p=0.0137; days to criterion (3 consecutive days above 70%): Control: (mean ± standard error of the mean, SEM) 5.35±0.27 days, hM4D: 7.05±0.51 days; unpaired t-test: $t=2.746$, $df=36$, **p=0.0094). No changes were seen in any other task variables, such as trial length, task latencies, or rewards consumed (supplemental Fig. 2, trial length: Control: 18.94±1.61 s, hM4D: 19.03±1.26 s; unpaired t-test: $t=0.04228$, $df=36$, $p=0.9665$; lever latency: Control: 4.932±0.199 s, hM4D: 5.372±0.252 s; unpaired t-test: $t=1.321$, $df=36$, $p=0.1949$; reward latency: Control: 0.5781±0.0143 s, hM4D: 0.5801±0.0125 s; unpaired t-test: $t=0.1086$, $df=36$, $p=0.9141$; rewards retrieved: Control: 99.78±0.05%, hM4D: 99.71±0.07%; unpaired t-test: $t=0.7668$, $df=36$, $p=0.4482$), suggesting that the impairments in performance were not due to a decrease in motivation or mobility.

Similarly, in a second cohort of mice tested in the ASST, we found that the mPFC-dependent EDSS was impaired in animals expressing hM4D compared with controls (Fig. 1e; n=14 Control animals, n=15 hM4D animals; Control: 10.57±0.42 days, hM4D: 15.07±1.79 days; unpaired t-test, $t=2.372$, $df=27$, *p=0.0251). Meanwhile, behavior in the non-mPFC-dependent initial acquisition portion of the set shifting task (IA) was unchanged (n=14 Control animals, n=16 hM4D animals; Control: 15.71±1.88 days, hM4D: 11.81±1.50 days; unpaired t-test, $t=1.639$, $df=28$, $p=0.1125$). No changes were seen in any other task variables, including IA or EDSS task latencies (supplemental Fig. 3, IA dig latency: Control: 24.29±5.84 s, hM4D: 32.47±8.91 s; unpaired t-test: $t=0.7448$, $df=28$, $p=0.4626$; SS dig latency: Control: 34.57±8.39 s, hM4D: 32.07±4.32 s; unpaired t-test: $t=0.2708$, $df=27$, $p=0.7886$).

These results indicate that adolescent thalamic inhibition results in long-term, persistent consequences to mPFC-dependent cognitive processes. To test whether adolescence is in fact a sensitive period, or

whether the circuit is sensitive to transient changes at any age, we also inhibited the thalamus for a comparable time window during adulthood, P90-120, and tested the long-term effects forty days later, at P160 (Figure 1f).

Adult thalamic inhibition affected neither acquisition of the NMS task (Fig. 1g, NMS acquisition: n=6 Control animals, n=10 hM4D animals; learning curve: 2-way rmANOVA, effect of time $F(5.501,77.01)=40.21$, $p<0.0001$, effect of group $F(1,14)=1.462$, $p=0.2467$, effect of group x time $F(17,238)=0.8680$, $p=0.6126$; days to criterion: Control: 7.33±0.67 days, hM4D: 7.40±1.02 days; unpaired t-test, $t=0.04654$, $df=14$, $p=0.9635$) nor trials to criterion in the EDSS task (Fig. 1h; EDSS: n=20 Control animals, n=17 hM4D animals; Control: 12.40±0.89 days, hM4D: 10.76±0.64 days; unpaired t-test, $t=1.442$, $df=35$, $p=0.1583$), supporting the hypothesis that adolescence is a sensitive period in which changes in thalamic activity influence the development of thalamo-mPFC circuit maturation.

Adolescent but not adult thalamic inhibition impairs prefrontal excitability

To determine whether thalamic inhibition during adolescence leads to long-lasting changes in mPFC circuit function, we used slice physiology to measure spontaneous excitatory and inhibitory activity in mPFC layer II/III pyramidal cells, which receive projections from the thalamus (Fig. 2a). Following adolescent thalamic inhibition, the frequency of spontaneous excitatory post-synaptic currents (sEPSCs) was reduced, while the sEPSC amplitude was unchanged (Fig. 2b, c; n=20 Control cells, n=24 hM4D cells; frequency: Control: 4.438±0.429 Hz, hM4D: 3.202±0.325 Hz; unpaired t-test, $t=2.337$, $df=42$, $*p=0.0243$; amplitude: Control: 28.71±2.57 pA, hM4D: 29.82±1.47 pA; unpaired student's t-test, $t=0.3881$, $df=42$, $p=0.6999$). This change in frequency, but not amplitude, suggests a decrease in the quantity or functionality of pre-synaptic excitatory inputs. In contrast, we found no changes in frequency or amplitude of spontaneous inhibitory post-synaptic currents (sIPSCs) (Fig. 2b, d; n=20 Control cells, n=21 hM4D cells; frequency: Control: 3.421±0.376 Hz, hM4D: 2.627±0.323 Hz; unpaired t-test, $t=1.606$, $df=39$, $p=0.1163$; amplitude: Control: 32.29±2.08 pA, hM4D: 31.03±1.84 pA; unpaired t-test, $t=0.4450$, $df=34$, $p=0.6592$) pointing to a selective decrease in mPFC excitation.

These effects were again selective to thalamic inhibition during adolescence as we found no changes in excitatory or inhibitory inputs to prefrontal pyramidal cells following chronic thalamic inhibition in adulthood (Fig. 2f, g; sEPSC: n=12 Control cells, n=12 hM4D cells; frequency: Control: 4.674±0.448 Hz, hM4D: 4.675±0.561 Hz; unpaired t-test, $t=0.001936$, $df=22$, $p=0.9985$; amplitude: Control: 27.78±1.68 pA, hM4D: 29.75±1.78 pA; unpaired t-test, $t=0.8048$, $df=22$, $p=0.4296$; sIPSC: n=12 Control cells, n=12 hM4D cells; frequency: Control: 3.775±0.506 Hz, hM4D: 2.825±0.625 Hz; unpaired t-test, $t=1.181$, $df=22$, $p=0.2501$; amplitude: Control: 25.49±0.82 pA, hM4D: 23.69±1.82 pA; unpaired t-test, $t=0.9030$, $df=22$, $p=0.3763$). These findings, consistent with the behavioral results, point to adolescence as a sensitive time period during which thalamic activity regulates the development of mPFC circuitry.

Adolescent thalamic inhibition decreases thalamic projections to the mPFC

We next aimed to discover whether decreased subcortical anatomical inputs may contribute to the decrease in sEPSC frequency measured in the mPFC following adolescent thalamic inhibition. To test this question, we injected a retrogradely transported fluorescent protein, GFP, into the mPFC of adult mice that had experienced adolescent thalamic inhibition. Three weeks later, we used stereology to calculate the density of retrogradely labelled neurons in the midline thalamus, as well as in the basolateral amygdala (BLA, Fig. 3a), an additional region that projects to layer II/III of the mPFC. After outlining the regions using DAPI staining, we found a decrease in the density of cells projecting from the thalamus to the mPFC (Fig. 3c; n=6 Control animals, n=7 hM4D animals; cell density: Control: 453.2±61.3 cells/mm^2, hM4D: 260.3±56.1 cells/mm^2; unpaired t-test, t=2.326, df=11, *p=0.0401; total area: Control: 5.539±0.232 mm^2, hM4D: 5.429±0.178 mm^2; unpaired t-test, t=0.3834, df=11, p=0.7087). In contrast, we found no change in the density of cells projecting from the BLA (Fig. 3d; cell density: Control: 602.4±61.1 cells/mm^2, hM4D: 578.5±61.0 cells/mm^2; unpaired t-test, t=0.2749, df=11, p=0.7885; total area: Control: 5.687±0.211 mm^2, hM4D: 5.432±0.163 mm^2; unpaired t-test, t=0.9713, df=11, p=0.3523), suggesting that there is no global competition between subcortical regions projecting to the mPFC, as has previously been seen in early postnatal lesion studies[37]. The difference in thalamic projections is maintained when the thalamus/BLA ratio is taken (Fig. 3e; cell density ratio: Control: 0.742±0.065, hM4D: 0.467±0.091; unpaired t-test, t=2.376, df=11, *p=0.0368; total area ratio: Control: 0.981±0.055, hM4D: 1.006±0.049; unpaired t-test, t=0.3471, df=11, p=0.7351), indicating that there is not an artificial effect caused by different injected viral volumes across animals and groups. We saw no change in overall cell density within the thalamus based on DAPI-positive cell counts (supplemental Fig. 9, cell density: Control: 13902±474 cells/mm^2, hM4D: 14642±1051 cells/mm^2; unpaired t-test, t=0.6050, df=11, p=0.5575), suggesting a loss of thalamic inputs to the mPFC rather than thalamic cells.

Enhancing thalamic excitability in the adult animal rescues the cognitive impairments induced by adolescent thalamic inhibition

The anatomical changes suggest that the circuit alterations are persistent. Previous work has shown that exciting the thalamus can enhance performance in prefrontal-dependent cognitive tasks including in a working memory and a 2-alternative forced choice task[26,30]. Moreover, it has been suggested that the thalamus may act as a non-specific amplifier of mPFC activity during the delay periods of those behaviors[26,28-31]. Even though our task does not include delays in which the trial-specific information must be kept online, we aimed to discover whether activation of the remaining thalamic inputs would still improve behavior and whether this amplification can overcome the developmental circuit abnormalities.

Therefore, we enhanced thalamic activity during the set shifting task using a stabilized step-function opsin (SSFO, Fig. 4a). To correct the impaired EDSS behavior, we activated the SSFO with a 5 second pulse (473nm, 4mW) before the start of the EDSS portion of the task (Fig. 4b). Because the SSFO will slowly inactivate over time, we repeated the 5 s pulse during the intertrial interval (ITI) every 30 minutes while the animal was engaged in the task.

We performed a crossover experiment where each animal performed the ASST twice, with and without SSFO activation, ten days apart. We replicated the behavioral deficit in the adolescent thalamus-inhibited animals when the SSFO was not active, and found that increasing thalamic excitability via SSFO activation during EDSS was sufficient to rescue the behavior of adolescent thalamic inhibition animals to control levels (Fig. 4d, n=10 Control animals, n=15 hM4D animals; 2-way rmANOVA; effect of group $F(1,23)=5.407$, $p=0.0292$, effect of light $F(1,23)=5.002$, $p=0.0353$, effect of virus x light $F(1,23)=5.002$, $p=0.0353$; Holm-Sidak post-hoc: Control Light OFF vs. ON $p>0.9999$, hM4D Light OFF vs. ON $^{**}p=0.0035$). The effects of SSFO activation did not persist from the first day of testing to the second testing day, and repeating the experiment did not influence behavior (2-way rmANOVA; effect of light $F(1,46)=6.302$, $p=0.0156$, effect of run day $F(1,46)=2.512$, $p=0.1199$, effect of light x day run $F(1,46)=1.364$, $p=0.2488$). These data give an important mechanistic insight: even though the sensitive period in the circuit occurs in adolescence, thalamo-mPFC circuitry can still be acutely manipulated in adulthood to rescue the behavioral deficits.

Oscillatory activity does not explain the behavioral deficits and rescue

In sum, developmental thalamic inhibition leads to altered prefrontal circuit function, which results in impaired EDSS behavior. This deficit is then rescued by acute thalamic activation. To better understand the network mechanisms driving these findings, we examined several metrics of mPFC activity during the behavior: local field potential (LFP) activity, single unit cellular activity, and neural ensemble activity.

Prior work, using the same set shifting task, identified an increase in the power of gamma frequency (40-90 Hz) oscillations in the mPFC before correct, but not incorrect, choices during the EDSS behavior[7]. Moreover, this correct trial induced gamma signal was attenuated in mice that performed poorly in this set shifting task following developmental inhibition of their prefrontal parvalbumin (PV) expressing interneurons[7]. Similarly, other studies have also highlighted the importance of mPFC interneuron activity and the associated changes in task-related gamma power in proper EDSS behavior[38-42].

Consistent with these prior results[7], we found that mPFC gamma power was increased specifically before the decision in correct trials compared with power in incorrect trials of control animals (Fig. 5a, d, Correct: 0.1774±0.0064; Incorrect: 0.1625±0.0066; linear mixed effects model: fixed effect (Trial Type), $^{****}p=5.1208e-05$). However, this difference in correct vs incorrect gamma power was still observed after adolescent inhibition of the MD, albeit with a smaller-appearing effect size (Fig. 5b, d, Correct: 0.1813±0.0048; Incorrect: 0.1765±0.0068; linear mixed effects model: fixed effect (Trial Type), $^{**}p=0.0014916$). Moreover, thalamic SSFO activation had no significant effect on mPFC gamma power (Fig. 5c, d, Correct: 0.1697±0.0043; Incorrect: 0.1652±0.0099; linear mixed effects model: fixed effect (Trial Type), $^{*}p=0.015341$). These results suggest that changes in gamma power do not explain the deficit in the behavioral performance in mice that experience adolescent thalamic inhibition.

Other cognitive tasks are known to generate thalamo-cortical oscillations in the beta frequency range (12-30 Hz)[26,27,33]. In the ASST, we recorded an increase in beta power during the trial compared to the inter-

trial interval (ITI, supplemental Fig. 4a, ITI: 0.1822±0.0042; Trial: 0.2044±0.0036; linear mixed effects model: fixed effect (Trial), p=3.2642e-16). This beta activation was equivalent across all trial types (supplemental Fig. 4e, Correct: 0.2052±0.0041; Incorrect: 0.2011±0.0075; linear mixed effects model: fixed effect (Trial Type), p=0.18827) and was not affected by the developmental manipulation (supplemental Fig. 4b, hM4D: ITI: 0.1866±0.0018; Trial: 0.2124±0.0022; linear mixed effects model: fixed effect (Trial), p=2.0872e-41). In addition, we found no changes in a variety of other physiological metrics, including thalamo-mPFC coherence in the beta frequency range across trial types (supplemental Fig. 4c,d,f, Control: ITI: 0.3890±0.0090; Trial: 0.4146±0.0080; linear mixed effects model: fixed effect (Trial), p=2.0137e-07; Correct: 0.4188±0.0092; Incorrect: 0.3984±0.0152; linear mixed effects model: fixed effect (Trial Type), p=0.72808; hM4D: ITI: 0.3968±0.0041; Trial: 0.4331±0.0044; linear mixed effects model: fixed effect (Trial), p=6.7099e-19) and phase-locking between mPFC cell firing and thalamic beta oscillatory activity (supplemental Fig. 5, Control: Correct PPC: 0.01575±0.00420; Incorrect: 0.01904±0.00642; paired t-test: t=0.4114, df=26, p=0.6841; hM4D: Correct: 0.01623±0.00441; Incorrect: 0.01205±0.00561; paired t-test: t=0.7443, df=21, p=0.4649).

Altogether, these data show that changes in oscillatory activity cannot explain the behavioral deficit in mice that experienced developmental thalamic inhibition. As a result, we next analyzed the activity of cells and neural ensembles in the mPFC.

Adolescent thalamic inhibition impairs the ability of adult mPFC neurons to encode task outcome

To determine whether thalamic inhibition may alter encoding of information within the mPFC, we analyzed the firing rates of single units in the mPFC (Fig. 6a). Overall single unit firing rates (FR) were not altered by either the developmental manipulation and or the SSFO rescue (Fig. 6b). Most mPFC units showed task-modulated activity with cells showing either enhanced or decreased activity during the EDSS task trials compared with the ITI (supplemental Fig. 6). During the trials, firing rates did not vary between groups (Fig. 6b, Control: 3.650±0.639 Hz; hM4D: 3.487±0.777 Hz; hM4D Light ON: 3.058±0.516 Hz; 1-way ANOVA, F(2,194)=0.2493, p=0.7796). Furthermore, FR did not significantly vary between different trial types, such as correct trials and incorrect trials (Fig. 6c, Control: FR during Correct: 3.570±0.647 Hz, Incorrect: 3.744±0.630 Hz; paired t-test: t=0.6546, df=71, p=0.5148). Thus, individual FR do not predict trial outcomes in control animals. Moreover, this metric was not affected by either developmental thalamic inhibition or acute thalamic activation (hM4D: Correct: 3.607±0.859 Hz, Incorrect: 3.676±0.873 Hz; paired t-test: t=0.3174, df=48, p=0.7523; hM4D Light ON: Correct: 3.058±0.519 Hz, Incorrect: 3.023±0.550 Hz; paired t-test: t=0.1539, df=70, p=0.8781). These findings were consistent, even when selecting only the task-modulated cells, or other subcategories, such as cells that increased their firing rates during the trial or cells that decreased their firing during the trial.

Behavioral outcomes may also be understood by analysis of multi-neuronal activity in the mPFC[43-45]. Previous studies have highlighted the benefits of analyzing firing rates across multiple neurons to better elucidate task behaviors, contexts, and outcomes[44]. We therefore chose to analyze the mPFC cell activity as a neural ensemble.

First, we were interested in the correlation between the firing of cells. We therefore analyzed cross-correlations between the firing of each cell, finding a peak correlation during the EDSS trials for each pair of cells. Adolescent thalamic inhibition reduced peak cross-correlations, and they were recovered following acute thalamic SSFO activation (Fig. 6d, Control: 0.0177±0.0430; hM4D: 0.0124 ±0.0212; hM4D Light ON: 0.0201±0.0414; linear mixed effects model, fixed effect of group: Control vs. hM4D: *p=0.041622; hM4D vs. hM4D Light ON: **p=0.0090838).

The increase in cross-correlations during incorrect over correct trials suggest a differential recruitment of neuronal ensembles during trials that have different outcomes. We therefore employed a linear decoder to elucidate differences in firing at the network-level (Fig. 6e). Taking the firing rates for all cells in an experimental group across all trials, we trained a linear decoding algorithm using 50% of all trials for each cell to predict whether the behavioral outcome would yield a correct or incorrect trial. We then tested the decoder on the other 50% of trials to determine whether we could predict trial outcome based on cell firing rates. To determine chance performance, we employed the same decoding algorithm using randomly shuffled trial outcomes, repeated 1000 times[46]. Employing this decoder on the control group showed a resulting performance that was significantly better than chance, at 74.71% accuracy (Fig. 6f, shuffled performance: 49.95±3.75%, ****p=3.9604e-11). This finding is eliminated following adolescent thalamic inhibition, where the decoder was no better than chance at 43.25% accuracy (shuffled performance: 51.13±7.49%, p=0.2926). Crucially, acute thalamic enhancement rescued the decoder performance to 69.41% accuracy (shuffled performance: 50.15±3.08%, ****p=3.9472e-10).

Of note, no subset of neurons contributed more to the decoder performance, with an even distribution across the populations in all three groups (supplemental Fig. 8a, b). Similarly, the decoding performance discrepancies across groups are visible with randomly selected subgroups of neurons. The pattern can be seen with as few as 5 neurons (supplemental Fig. 8c, 2-way rmANOVA Holm-Sidak post-hoc for each chunk, analysis with 5 neurons: Control vs. hM4D: p<0.0001, Control vs. hM4D Light ON: p=0.1557, hM4D vs. hM4D Light ON: p<0.0001). Moreover, the control decoding performance was not seen when applied to trials in the IA portion of the ASST (supplemental Fig. 8d, Control: 50.35%, shuffled data: 50.13±3.14%, p=0.9438), indicating the specificity of the role of the mPFC during the EDSS.

Together, these findings show that adolescent thalamic inhibition disrupts prefrontal encoding of EDSS task outcome in adulthood via decreasing correlated activity between prefrontal neurons. This disruption can be rescued by acute thalamic activation during adulthood.

Discussion

Adolescence is a sensitive period for the development of thalamo-mPFC circuitry

Thalamic input activity has been shown to be important for sensory cortex maturation, including the visual cortex[1,3–5]. More recent studies have also begun to explore how neuronal activity shapes the

development of higher cognitive structures, such as the medial prefrontal cortex (mPFC)[7–9]. Primarily, these studies have focused on changes to intrinsic components of mPFC circuitry, such as interneuron or layer II/III pyramidal neuron activity[7,10,47]. Some have also highlighted similarities between mechanisms found in sensory sensitive periods and mPFC adolescent development, including BDNF expression, NMDA receptor changes, and the formation of perineuronal nets[48–51]. This paper is the first to explore whether afferent input from the thalamus shapes cortical maturation and whether inhibition of thalamic activity leads to long-lasting changes in mPFC function and behavior.

We found that thalamic inhibition during adolescence leads to persistent impairments in mPFC circuit function and cognitive behaviors in adulthood. Specifically, we observed impairments in two mPFC-dependent behavioral tasks assessing the acquisition of a non-match to sample rule and attentional set shifting. These changes were associated with a decrease in cortical excitability. We determined that adolescence is a sensitive period because the impairments in behavior and excitability were not observed following a comparable thalamic inhibition during adulthood. These results indicate that excitatory activity from the thalamus during adolescence is essential for mPFC development. This mirrors the findings in sensory sensitive periods, where thalamo-cortical inputs are compromised following sensory deprivation, ultimately leading to cortical restructuring[2,3,52].

Adolescence is a key period of cortical maturation

While sensitive periods in sensory systems often occur during very early postnatal development[3–5], we found that adolescence is a sensitive period for mPFC development. Adolescence is known to be a period of vulnerability in the development of psychiatric disorders such as schizophrenia in humans[11–13, 53]. Moreover, functional imaging studies have shown that thalamo-prefrontal hypoconnectivity, a finding in patients with schizophrenia, is already present in young adolescents at clinical high risk for the disorder[15,18–23]. We chose to inhibit thalamic activity in mice during the P20-50 window because it is known that the mPFC is maturing during this time[38,54–62]. In rodents, the volume of the mPFC peaks around P24 after which point it decreases, reflecting a period of dendritic pruning in mPFC pyramidal neurons, which peaks around P30[63–66]. It has been postulated that this volumetric change and pruning could result in part from refinement of thalamo-cortical synaptic contacts during this period[67]. Furthermore, one classical hypothesis originally presented by Feinberg states that in schizophrenia aberrant activity-dependent pruning during adolescence may lead to persistent changes in prefrontal circuit function[14]. Although we did not study the effects of thalamic inhibition on cortical pruning, we show that decreased thalamic input activity is important for cortical circuit maturation. Future studies should address how much altered pruning contributes to the anatomical and slice physiological changes described here.

In addition to dendritic pruning, the mPFC also undergoes changes in myelination and interneuron development, which together promote emergent changes in network activity and behavioral functionality[54,55,68]. Therefore, the P20-50 window represents a possible period of heightened thalamo-

cortical projection refinement in normal development, which may in turn affect multiple other components of prefrontal development.

Our work does not explain how thalamic inhibition immediately alters mPFC function during adolescence, as we focused on the long-term consequences measured in the adult animal. Other recent studies have explored homeostatic plasticity in sensory systems following changes in activity[69,70]. They found that different forms of plasticity (e.g. changes in intrinsic excitability and synaptic excitation and inhibition) occur at different developmental stages. However, these effects on plasticity were only analyzed within 1 or 2 days after the change in activity, and the persistence of these effects remains unknown. Future studies will address the immediate plasticity mechanisms in the mPFC that are induced by midline thalamic inhibition during adolescence.

Adolescent thalamic inhibition impairs thalamo-cortical projections

Thalamic projections to the mPFC are a crucial source of excitatory input to mPFC pyramidal cells. Following adolescent thalamic inhibition, we found reduced mPFC pyramidal excitability in adulthood. Due to the reduction in spontaneous excitatory post-synaptic current frequency, but not amplitude, we hypothesized that this change was primarily driven by a reduction in pre-synaptic inputs and that decreased inputs from the thalamus may contribute to this change.

We were able to confirm this hypothesis through retrograde labelling. Adolescent thalamic inhibition led to a reduction in thalamo-mPFC projection cell density. However, this intervention had no effect on mPFC-projecting cells from other subcortical regions, such as the BLA, indicating specificity to thalamo-cortical projections. This result is distinct from what has been observed after early developmental subcortical lesions, which showed a compensatory increase in BLA-mPFC projections following early postnatal (P7) ventral hippocampal lesions[37]. We believe this thalamo-mPFC projection reduction is due to a decrease in axonal arborization rather than thalamic cell numbers because DAPI staining in the thalamus was unchanged (supplemental Fig. 9). Moreover, before adolescence, the thalamus has already undergone a period of heightened apoptosis around P13, further supporting the notion that inhibiting the thalamus during adolescence comes primarily at a period of thalamo-cortical synaptic refinement[67,71]. Since we used bilateral injections of retrograde virus to investigate the impact of developmental thalamic inhibition on cortical projections, we were unable to determine whether there were any changes to cortico-cortical contralateral projections. Future studies could examine whether intra-cortical connectivity is also affected.

We demonstrated that non-specific acute thalamic activation in adulthood following adolescent thalamic inhibition was sufficient to rescue the behavioral cognitive deficit. However, we also found that this restored cognitive ability was not long-lasting as there was no residual effect 10 days following the thalamic activation. Thus, it is unlikely that a one-time thalamic activation is sufficient to regrow the lost

thalamic inputs. Rather, it simply boosted activity of the remaining thalamic projections, further pointing to a non-specific role for these inputs.

Task-evoked oscillatory activity cannot explain the behavioral outcomes

Previous studies have shown the importance of task-induced gamma for predicting behavioral performance during EDSS and that this signal can be persistently disrupted following adolescent inhibition of mPFC PV interneurons[7]. Here, we also found that mPFC gamma power was correlated with behavioral performance in control animals, with elevated gamma in correct trials compared with incorrect trials, but this pattern was not affected adolescent thalamic inhibition. Consistent with the unchanged gamma power in developmental thalamic inhibition mice, we did not find any deficits in cortical inhibition in adult mice that experienced adolescent thalamic inhibition, as was observed following adolescent PV inhibition[7]. This suggests that the long-term consequences of adolescent thalamic inhibition may not necessarily involve cortical PV interneurons.

Beta oscillatory activity has also previously been identified in thalamo-prefrontal manipulations, often in the context of working memory behaviors[26,33]. While we did find task-induced beta oscillations, these were not correlated with behavioral outcome in controls and not affected by adolescent thalamic inhibition.

Altogether, these data suggest that, despite reduced thalamic inputs to the mPFC, oscillatory measures of the thalamo-mPFC circuitry cannot explain the deficits observed during the EDSS behavior following adolescent thalamic inhibition. Thus, while these oscillations may be necessary for the proper execution of this task, they are not the only mechanism at play.

The thalamus supports local mPFC encoding of behavioral trial outcomes

To determine whether adolescent thalamic inhibition disrupts single unit activity in the adult animal, we examined average mPFC cell firing rates during EDSS trials but found no changes in individual neuron firing rates across different trial types. However, recent theories suggest that multiple neurons can form ensembles that determine functional properties and outcomes, in ways beyond single neuron firing[43,44]. When we studied the cross-correlations between cell pairs, we found that cross-correlations were disrupted following adolescent thalamic inhibition. This disruption was rescued by acute thalamic activation, pointing to a role of thalamic inputs in enhancing mPFC cellular communication.

To further explore the effects on population encoding, we trained a linear decoding algorithm using a subset of trials to predict the EDSS trial outcome based on mPFC neuronal ensemble activity. Using this decoder, we were able to accurately predict trial outcome in control animals, but the decoding ability was entirely lost following adolescent thalamic inhibition. Importantly, mPFC neurons regained the ability to

encode task outcome after thalamic stimulation, suggesting that thalamic excitation rescues outcome encoding and task performance.

Other thalamo-cortical circuits, namely in motor circuitry, have shown a task-specific role for both thalamic and cortical activity[72]. In addition, modifying activity of different mPFC cell types have also demonstrated task-specific roles for mPFC cellular subpopulations[73]. Meanwhile, thalamic input to the mPFC has been hypothesized to non-specifically amplify or sustain local mPFC connectivity and encoding[28–30]. This study points to a role of the thalamus as a non-specific amplifier of mPFC cellular encoding during this cognitive flexibility task in two major ways. First, adolescent thalamic inhibition disrupted thalamo-mPFC projections in adulthood, which coincides with both reduced mPFC cellular cross-correlations and disrupted mPFC task outcome encoding. Second, non-specific thalamic activation, even in the context of fewer thalamic projections, during the EDSS was sufficient to restore these cross-correlations and outcome-specific mPFC activity.

The mPFC itself has been intensively studied in cognitive flexibility tasks, such as the ASST. Some studies have pointed to the post-decision period as a crucial point for the mPFC during the EDSS[41,74]. While we found mPFC encoding throughout the trial, the decoder performed better when using post-decision versus pre-decision period firing activity within a trial, indicating that the mPFC may indeed be particularly important in the period following the choice.

Acute thalamic enhancement following developmental inhibition offers great promise for therapeutic interventions

Following thalamic inhibition during adolescence, we found persistent anatomical changes in thalamic projections to the mPFC. Nevertheless, we were able to rescue the behavioral deficits by acutely enhancing activity in the thalamic in the adult mouse, even though this manipulation is unlikely to reverse the anatomical changes. It has previously been shown that enhancing thalamic excitability during the delay of a prefrontal-dependent working memory and a 2AFC task enhanced performance in both tasks[26,30]. Our data suggest that the thalamus plays a broader function in amplifying mPFC activity that is not restricted to delay-response tasks but also other cognitive processes. This result offers a major insight into potential therapeutic interventions in this circuit, as it indicates that even with persistent changes in circuit anatomy, a relatively non-specific thalamic excitation may still be able to improve behavior. Human imaging studies have pointed to the importance of the thalamo-prefrontal connectivity in cognitive functioning[18–21]. In patients with schizophrenia, deficits in cognition have been related to hypoconnectivity between the thalamus and PFC, which is already seen in young adolescents before their diagnosis[15,22,23]. Given the relevance of thalamo-prefrontal circuitry in psychiatric disorders like schizophrenia, this study offers key mechanistic insights into the etiology of, and potential therapies for, these disorders.

Methods

Animal Husbandry. All animal procedures were done in accordance with guidelines derived from and approved by the Institutional Animal Care and Use Committees at Columbia University and the New York State Psychiatric Institute. Animals were housed under a 12 h light-dark cycle in a temperature-controlled environment with food and water available ad libitum, unless otherwise noted. Heterozygous GBX2-CreERT (Jackson Labs, Stock #022135) males, back-crossed for at least 5 generations, were bred with C57/Bl6 females (Jackson Labs, Stock #000664) to produce offspring that were used in all experiments. At postnatal day 10 (P10), tail samples were collected from offspring to genotype (Transnetyx, Inc). At P13, GBX2-CreERT heterozygous offspring were used for viral injections. These mice were housed in cages with the mother and littermates. At P15 and P16, all offspring were given intraperitoneal (i.p.) injections of tamoxifen (Sigma-Aldrich, T5648), dissolved in corn oil, at 75 mg/kg. All offspring were weaned at P28, and GBX2-CreERT heterozygotes were kept for experiments and group housed with same-sex littermates (5 mice/cage).

For midline thalamic inhibition, mice were given i.p. injections of clozapine-N-oxide (CNO), dissolved in 0.9% saline, at 1 mg/kg, twice per day. These injections took place every day P20-50 for adolescent inhibition and P90-120 for adult inhibition.

At P70, mice used for cell density studies were injected with virus, and mice used for *in vivo* optogenetic neurophysiology recordings during behavioral experiments were virally injected and implanted with optrodes. Implanted mice were subsequently housed in cages of 2–3 mice/cage.

All behavioral testing and *in vivo* recordings were done 40 days after the last CNO injection in adult mice (> P90). During behavioral training and testing, mice were food-restricted and maintained at 85% of their initial weight.

Surgical procedures. For the viral injections at P13, mice were anesthetized with ketamine (4 mg/ml) and xylazine (0.6 mg/ml) and head-fixed in a stereotactic apparatus (Kopf). Mice were injected bilaterally in the midline thalamus with AAV5-hSyn-DIO-hM4D-mCherry (Addgene #44362) or a control virus, either AAV5-hSyn-DIO-EGFP (Addgene #50457) or AAV5-hSyn-DIO-mCherry (Addgene #50459) at a volume of 0.25 µl (0.1 µl/min). The juvenile midline thalamus coordinates used were: -1.0 AP, ± 0.25 ML, -3.0 DV (skull at bregma).

For the cell density study surgeries at P70, mice were anesthetized with ketamine (10 mg/ml) and xylazine (1 mg/ml) and head-fixed in a stereotactic apparatus (Kopf). Mice were injected bilaterally into the mPFC with retrograde AAV-CAG-GFP (Addgene #37825) at a volume of 0.25 µl (0.1 µl/min). The mPFC coordinates used were: +1.8 AP, ± 0.35 ML, -2.5 DV (skull at bregma).

For the *in vivo* optogenetic neurophysiology experiments, mice were anesthetized with isoflurane and head-fixed in a stereotactic apparatus (Kopf). All mice were injected bilaterally into the midline thalamus with AAV5-CaMKII-hChR2(C128S/D156A)-EYFP (University of North Carolina Vector Core) at a volume of 0.4 µl (0.1 µl/min). The midline thalamus coordinates used for the viral injection were: -1.2 AP, ± 0.35 ML, -3.2 DV (skull at bregma). During the same procedure, mice were also implanted with an optrode,

consisting of a 36-channel narrow electronic interface board (Neuralynx, Bozeman, MT), a single stereotrode bundle, additional local field potential (LFP) wires, and 2 flat tipped, ferrule-coupled optical fibers (0.22 NA, 200 µm diameter). Stereotrodes for recording spikes were made from 13 µM tungsten fine wire (California Fine Wire, Grover Beach, CA) and were coupled to one 50 µM tungsten wire for recording LFPs. This stereotrode bundle was then unilaterally targeted to the left mPFC. Another 50 µM tungsten wire was glued to the left optical fiber, extending 450 µm below the bottom of the fibers. Both fibers and the wire were implanted into the midline thalamus. For signal processing, skull screws placed over the cerebellum and olfactory bulb served as ground and reference, respectively, while spikes were referenced to a local mPFC stereotrode wire. Coordinates were as follows: mPFC: +1.85 AP, -0.35 ML, -1.4 DV (brain); midline thalamus: -1.2 AP, ± 0.3 ML, -2.7 DV (brain).

All coordinates are in mm relative to bregma (AP, ML) and skull or brain surface (DV) where specified.

Behavioral procedures. All behavioral tasks were conducted during the light cycle. At P90, mice were gradually restricted to 85% of their body weight.

Non-Match to Sample working memory task: The task was conducted as previously described in Benoit et al, 2020[34]. Eight identical operant-conditioning chambers (ENV-307A; Med Associates, Georgia, VT) were used. The chamber measured 15.24 cm long x 13.34 cm wide x 12.7 cm high. Each chamber was housed in a sound-attenuated box and equipped with two retractable levers (ENV-312-3M) on the front wall (the 13.34 cm side), with one milk dipper between them (ENV-302RM-S, Fig. 2a). The back wall contained one noseport (ENV-313M) directly opposite to the milk dipper, which delivers 1 drop of evaporated milk (0.01 ml). A 1.0 A house light was positioned directly above the noseport. A computer (COM-106-NV, Intel i5-7400) controlled and recorded all experimental events and responses via an interface (MED-SYST-16e-V). Med-PC V programs were used to administer and record the task. Mice were shaped to the different parts of the operant task. They were first given 2 days of habituation to the milk dipper, followed by 7 days of training to associate a lever press with a milk reward. Lastly, they were given 5 days of noseport training before beginning the acquisition stage of the behavior.

During acquisition, each trial began with the house light being turned on and an illuminated noseport to signal an initial noseport entry. The first noseport entry triggered the start of the sample lever presentation. During the sample phase, only one lever was presented in a pseudo-random order. After the sample lever press, the noseport was immediately re-illuminated (following a 0 second delay) signaling a second noseport entry. Following the second noseport entry, the choice phase began, and both levers were presented. If the animal pressed the opposite lever to the sample lever of that trial (non-match), the trial was recorded as “correct” and a dipper reward was given. If the animal pressed the same lever as the sample, the trial was recorded as “incorrect” and the dipper was not presented. This final step was followed by a 10 second inter-trial interval (ITI) during which the house light was turned off.

Acquisition was repeated every day with 120 trials per day; 60 trials with each lever presented as the sample, in a pseudo-random order. For this experiment, pseudo-random refers to a random distribution

with the restriction that the same condition cannot be presented for more than 2 consecutive trials. Beginning on day 6 of acquisition, mice had a 5-second time limit in which to make the second noseport entry. This restriction allowed us to shape the animals' behavior to ensure a standardized length of delay between subjects. If the animal did not make a noseport entry in the time allotted, the trial was aborted and was omitted from the calculations. For the final 3 days of acquisition, the total number of trials was increased to 160 trials. Throughout the experiment, mice were given unlimited time to complete the required trials.

During the acquisition stage, all mice achieved a criterion level of performance, defined as 3 consecutive days above 70% correct.

Attentional Set Shifting cognitive flexibility task: The task was conducted as previously described in Canetta et al, 2016[75]. Mice were first habituated to the testing arena on day 1. On days 2–3, they were trained to dig in both bedding media (corn cob and paper pellet, both unscented) to obtain a food reward. Once the animals dug reliably when presented with both types of bedding, testing began. For each trial, mice were placed at the opposite end from 2 terra cotta pots containing different odor/medium combinations. For initial acquisition (IA), mice needed to learn that the cinnamon scent, not the paprika scent, predicted a Honey Nut Cheerio reward, irrespective of the bedding media. For the first 5 trials, mice could explore both pots until they found the reward, but the trial was only scored as correct if the animal initially chose the correct pot. From the 6th trial onward, once the mouse began digging in a pot, the entrance to the area containing the other pot was closed off. Criterion was reached when the mouse made eight of ten consecutive correct choices. If the mouse did not meet criterion in 30 trials, the animal did not advance to the next stage (one animal from the adolescent manipulation hM4D group did not meet the IA criterion). If the mouse did reach criterion, extra-dimensional set shifting (EDSS) began. In the EDSS portion of the task, the animal needed to learn that the type of bedding medium (paper pellets, not corn cobs) predicted the Honey Nut Cheerio reward, irrespective of odor. Criterion was reached when a mouse made eight of ten consecutive correct choices.

For optogenetic experiments, mice completed the task twice, 10 days apart. Animals were randomized to receive the light ON or OFF on Run Day 1 or Run Day 2 during the EDSS portion of the task. For Run Day 1, the rules in the IA and the EDSS were as described above, with odor (cinnamon rewarded) predicting the reward in the IA and texture (paper rewarded) predicting the reward in the EDSS. For Run Day 2, the rule in the IA was the same as the EDSS for Run Day 1, with paper rewarded. The rule in the EDSS for Run Day 2 was odor predicting the reward, with paprika rewarded. For the EDSS on the second run, mice that previously had the light ON for Run Day 1 had the light OFF and vice versa. There was no effect of Run Day on overall performance; therefore, the light conditions could be pooled across runs for analysis.

Optogenetic Parameters. In optogenetic stabilized step-function opsin (SSFO) experiments, for the light ON run, a 5 s blue light pulse (473 nm, 4 mW) was used for opsin activation prior to the first EDSS trial. The light was delivered via flat tipped 200 μm diameter, 0.22 NA fiber optics. To ensure continued opsin activation throughout the EDSS trials, the 5 s pulse was repeated between trials every 30 min.

Slice Electrophysiology. Whole-cell current and voltage clamp recordings were performed in layer 2/3 mPFC pyramidal cells and midline thalamic cells. Recordings were obtained with a Multiclamp 700B amplifier (Molecular Devices) and digitized using a Digidata 1440A acquisition system (Molecular Devices) with Clampex 10 (Molecular Devices) and analyzed with pClamp 10 (Molecular Devices). Following decapitation, 300 μM slices containing mPFC or midline thalamus were incubated in artificial cerebral spinal fluid (ACSF) containing (in mM) 126 NaCl, 2.5 KCl, 2.0 $MgCl_2$, 1.25 NaH_2PO_4, 2.0 $CaCl_2$, 26.2 $NaHCO_3$, and 10.0 D-Glucose, bubbled with oxygen, at 32°C for 30 minutes before being returned to room temperature for at least 30 minutes prior to use. During recording, slices were perfused in ACSF (with drugs added as detailed below) at a rate of 5 mL/min. Electrodes were pulled from 1.5 mm borosilicate-glass pipettes on a P-97 puller (Sutter Instruments). Electrode resistance was typically 3–5 MΩ when filled with internal solution consisting of (in mM): 130 K-Gluconate, 5 NaCl, 10 HEPES, 0.5 EGTA, 2 Mg-ATP, and 0.3 Na-GTP (for thalamic recordings; pH 7.3, 280 mOsm) or 130 mM Cs-Gluconate, 10 HEPES, 2 MgCl2, 0.2 EGTA, 2.5 MgATP, 0.3 NaGTP, and 5 Lidocaine N-ethyl bromide (for pyramidal cell recordings; pH 7.3, 280 mOsm).

Midline thalamic recordings: Animals were sacrificed at P35 or P105 after either receiving CNO for 2 weeks or not. hM4D (mCherry-tagged) or GFP-infected thalamic cells were identified by their fluorescence at 40x magnification under infrared and diffusion interference contrast microscopy using an inverted Olympus BX51W1 microscope coupled to a Hamamatsu C8484 camera. Intrinsic and active membrane properties (resting membrane potential, input-output firing frequency curve) were recorded in current clamp using the K-Gluconate intracellular solution detailed above before and after 10 μM CNO was bath applied to the slice.

mPFC recordings: Animals were sacrificed for recordings at P90 for the adolescent manipulation or P160 for the adult manipulation. mPFC pyramidal cells were visually identified based on their shape and prominent apical dendrite at 40x magnification under infrared and diffusion interference contrast microscopy using an inverted Olympus BX51W1 microscope coupled to a Hamamatsu C8484 camera. Spontaneous excitatory post-synaptic currents (sEPSCs) were recorded in voltage clamp at a holding potential of -55 mV and spontaneous inhibitory post-synaptic currents (sIPSCs) were recorded in voltage clamp at a holding potential of + 10 mV. 60 seconds of the current recording for each condition was analyzed. Recordings were filtered with an eight-pole low-pass Bessel filter, and sEPSCs and sIPSCs were detected using MiniAnalysis (Synaptosoft). All event data was averaged by cell.

In vivo electrophysiology. *In vivo* electrophysiology recordings were performed while the animals were performing the attentional set shifting task. Field potential signals from the mPFC and midline thalamus were referenced against a screw implanted in the anterior portion of the skull above the olfactory bulb. Recordings were amplified, band-pass filtered (1-1000 Hz LFPs; 600–6000 Hz spikes) and digitized using a Digital Lynx system (Neuralynx). LFPs were collected at 2kHz, while spikes were detected by online thresholding, collected at 32 kHz, and sorted off-line. TTLs were manually inserted to record the timing of relevant events (e.g., trial start, decision point, trial end).

Histology. Adult mice were deeply anesthetized with 100 mg/kg ketamine and 5 mg/kg xylazine (i.p.). For *in vivo* electrophysiology experiments, electrolytic lesions were induced at each recording site by passing current (50 μA, 30 s) through electrodes prior to perfusion. All animals were perfused with phosphate-buffered saline (PBS) followed by 4% paraformaldehyde in PBS. Brains were dissected out and post-fixed in 4% PBS overnight before being transferred to 1% PBS for long-term storage. Brains were sectioned serially at 40 μm for cell density studies, and 50 μm for all other experiments, on a vibratome (Leica, Buffalo Grove, IL, USA). The following primary antibodies were used: mCherry (rabbit-anti-dsred; Takara Bio, Mountainview, CA, USA; 632496, 1:250) or green fluorescent protein (GFP; Abcam, Cambridge, UK, ab13970, 1:1000). Primary antibody incubation was 48 hours at 4˚C. Alexa Fluor-conjugated secondary antibodies (Invitrogen, 1:1000) were used for secondary detection. Stained tissue slices were then mounted on slides with Vectashield mounting medium containing DAPI (Vector Labs). Viral expression was confirmed from mCherry or GFP staining, and locations of recording site lesions were confirmed under DAPI.

Stereology was used to assess retrogradely-labeled cell numbers in the midline thalamus and BLA in adult developmental manipulation and control animals for the cell density studies using StereoInvestigator software (MBF Biosciences, Williston, VT, USA). Every 3rd slice was used, and regions were traced using DAPI staining. During image acquisition and quantification, the investigator was blind to the treatment.

LFP and single-unit analysis. Neuralynx files containing LFP and spike data were imported into Matlab with Neuralynx MATLAB import/export package v 4.10.

LFP samples were notch filtered using the MATLAB Chronux package to remove 60 cycle noise (http://chronux.org/; rmlinesmovingwinc.m). Mechanical artifacts were eliminated by removing samples whose voltage was more than 3 standard deviations from the entire signal mean. The cleaned signal was then root-mean-squared. Power and coherence were calculated using the wavelet transformation package in MATLAB. These values were averaged over the relevant time windows (e.g., 6 s before the decision point). Frequency ranges were as follows: 40–90 Hz for gamma, 12–30 Hz for beta.

Single units were automatically clustered using Klustakwik (Ken Harris) based on spike sorting of the first two principal components, peak voltage and energy from each stereotrode channel. Clusters were then accepted, merged or removed based on isolation distance, visual inspection of feature segregation, inter-spike interval distribution, cross-correlation in spike timing for simultaneously recorded units, and stability across the recording session. From recordings during the optogenetic experiment, we isolated 75, 55, and 69 single units from the control, hM4D, and hM4D light ON groups, respectively.

To analyze the phase-locking of single cells in the mPFC with the LFP in the thalamus in the beta range, we calculated the pairwise phase comparison (PPC)[76] of mPFC spikes to thalamic LFP. The LFP signal was first digitally bandpass-filtered (12–30 Hz) using a zero-phase-delay filter (filter0, K. Harris and G. Buzsaki), and the Hilbert transform of the bandpass-filtered signal was calculated to obtain the

oscillatory phase. The magnitude of the phase-nonuniformity of spike times relative to the filtered LFP oscillation was then calculated for the 6 s before the decision point in correct and incorrect trials. Of note, we chose the period before the decision point given previous findings in that window[7]. However, we found similar results when looking in the 6 s period after the decision point or the full 12 s window. In order to avoid spuriously high or low PPC values, only units that fired at least 50 spikes in each condition were used.

Statistics. Statistical analysis and graph preparation for all data was done with Prism 9 software (Graphpad Software, San Diego, CA, USA) or custom scripts in MATLAB (Mathworks, Natick, MA, USA) and Python. One-way ANOVA, two-way repeated measures ANOVA, and unpaired or paired two-tailed t-tests were used to analyze slice physiology, behavior, cell density, and single unit firing rates. For the slice physiology acute CNO experiment, Holm-Sidak post-hoc analyses were used to compare the hyperpolarization upon bath application of CNO for all hM4D groups to the control. For the optogenetic behavior, Holm-Sidak post-hoc analyses were used to compare light off vs. light on outcomes.

To analyze differences in gamma power for each group, we fit linear mixed models with gamma power as outcome. The random effect was animal, and the fixed effect was either trial (ITI vs. trial) or trial outcome type (correct vs. incorrect). Power as a function of frequency was plotted by averaging the gamma power across the 6 s before the decision point. Mean power or coherence was calculated for those 6 s for the range of 40–90 Hz for gamma, or 12–30 Hz for beta. Of note, we chose the period before the decision point given previous findings in that window[7]. However, we found similar results when looking in the 6 s period after the decision point or the full 12 s window.

For all cells for each experimental group, firing for all cells were binned into 50 ms windows. These firing rates were then smoothed by taking the average firing rate of the surrounding 5 bins (i.e., 250 ms). These smoothed firing rates were then used in the subsequent analyses, where indicated.

To represent z-scored firing rates, the mean and standard deviation was calculated for the firing rate for all EDSS ITI time bins. The smoothed firing rates for each time bin for the 12 s surrounding the decision in each trial were calculated using the ITI mean and standard deviation. The mean z-score was then taken across all trials for each time bin.

Mean firing rates were taken for each cell across the 12 s surrounding the decision of each trial. Mean firing rates were calculated first for all trials. Then, the mean firing rate was taken for each trial outcome type (correct vs. incorrect). Paired t-tests were used to compare the firing rates across trial types.

For cross-correlations, firing rates were binned into 50 μs windows. For each trial, the 12 s surrounding the decision point was taken, and the spike train for each trial was concatenated with the trains for that cell and trial outcome type. The firing for each spike train was normalized to overall firing rate, and the Matlab function, xcorr, was then applied to all pairs of cells within each animal, using a maximum lag time of ± 80 ms. The peak cross-correlation value for each cell pair was used in the analysis, with each cell pair having a peak cross-correlation during correct and incorrect trials. We then fit a linear mixed model with

peak cross-correlation as outcome, fixed effects of group (control, hM4D, hM4D Light ON) and trial outcome type (correct vs. incorrect), and random effects of animal and cell. Of note, because the analysis requires cell pairs, certain animals were removed from the analysis if they had only one isolated cell (Control: 2 eliminated animals; hM4D: 3; hM4D Light ON: 2).

Decoder. The linear decoder was custom-written using Python. The smoothed firing rates for the 12 s around the decision (described above) were used for each trial, and the trial outcome (i.e., correct or incorrect) was also used in the decoder. The analysis was done using the trials from the EDSS (Fig. 6f) or the IA portion of the task (supplemental Fig. 8d). Of note, certain animals were removed from the analysis if they had fewer than 2 neurons or fewer than 2 of each trial outcome (EDSS: Control: 4 eliminated animals; hM4D: 5; hM4D Light ON: 4; IA: Control: 5).

The neural decoder algorithm was based on linear classifiers trained on pseudo-simultaneous population activity created by combining 50 ms-binned neural patterns recorded from different animals performing the same behavioral task. The decoding algorithm was cross-validated and tested against a null model with shuffled trial condition labels.

Cross-validation: We computed the decoding performance using a 20-fold cross validation (CV) scheme.

For each CV fold, we randomly selected half of the trials of each condition and used them to build pseudo-simultaneous (PS) activity (see below) which was used to train a Support Vector Machine (SVM) with a linear kernel to classify PS patterns into one of the two conditions.

Similarly, the remaining half of the trials were used to build PS activity that was used to test the trained SVM. The decoding performance was then assessed as the mean accuracy on the test set over the CV folds.

Pseudo-population: To build pseudo-populations, we randomly selected 50 ms binned neural patterns from training and testing trials of all animals and concatenated them to form a larger pseudo-simultaneous neural pattern. To obtain the training and testing data sets used in the cross-validation scheme, this procedure was repeated 10 x N times per condition, where N is the total number of neurons.

n-timebins decoding: To increase the signal to noise ratio of the decoder, we used a procedure where the decoder is trained to classify groups of n time bins sampled from the two conditions ($n = 1$ corresponding to standard single time-bin decoding). In practice, this was done when building pseudo-population activity by randomly sampling n different time bins for each individual animal to build a single pseudo-simultaneous time bin. Unless specified otherwise, we used $n = 5$.

Null model and p-value: All decoding performance values were tested against M repetitions of a null model by shuffling the condition labels of individual trials. After each shuffle of the labels, the exact same decoding procedure described above was repeated on the shuffled data. Unless specified otherwise, we used $M = 1000$. The p-value associated to the decoding performance was computed by comparing the performance of the shuffled model to the performance of the data.

Implementation: The analysis was performed in Python3 by using the *decodanda* package [link] and the *sklearn* implementation of SVM classifier [link].

Declarations

Data availability. The data that support the findings of this study are available from the corresponding author upon reasonable request.

Code availability. Med-PC V, MATLAB, and Python code used for administering the behavior and analysis of the data that support the findings of this study is available from the corresponding author upon reasonable request.

Acknowledgments

Author information removed.

Author contributions

Author information removed.

Competing Financial Interests

The authors declare no competing financial interests.

References

1 Takesian, A. E. & Hensch, T. K. Balancing plasticity/stability across brain development. *Prog Brain Res* **207**, 3-34, doi:10.1016/B978-0-444-63327-9.00001-1 (2013).

2 Hensch, T. K. Critical period regulation. *Annual review of neuroscience* **27**, 549-579, doi:10.1146/annurev.neuro.27.070203.144327 (2004).

3 Wiesel, T. N. & Hubel, D. H. Single-Cell Responses in Striate Cortex of Kittens Deprived of Vision in One Eye. *J Neurophysiol* **26**, 1003-1017, doi:10.1152/jn.1963.26.6.1003 (1963).

4 de Villers-Sidani, E., Chang, E. F., Bao, S. & Merzenich, M. M. Critical period window for spectral tuning defined in the primary auditory cortex (A1) in the rat. *J Neurosci* **27**, 180-189, doi:10.1523/JNEUROSCI.3227-06.2007 (2007).

5 Caras, M. L. & Sanes, D. H. Sustained Perceptual Deficits from Transient Sensory Deprivation. *J Neurosci* **35**, 10831-10842, doi:10.1523/JNEUROSCI.0837-15.2015 (2015).

6 Sun, Y. J., Espinosa, J. S., Hoseini, M. S. & Stryker, M. P. Experience-dependent structural plasticity at pre- and postsynaptic sites of layer 2/3 cells in developing visual cortex. *Proc Natl Acad Sci U S A* **116**,

21812-21820, doi:10.1073/pnas.1914661116 (2019).

7 Canetta, S. E. *et al.* Mature parvalbumin interneuron function in prefrontal cortex requires activity during a postnatal sensitive period. *bioRxiv*, 2021.2003.2004.433943, doi:10.1101/2021.03.04.433943 (2021).

8 Bitzenhofer, S. H., Pöpplau, J. A., Chini, M., Marquardt, A. & Hanganu-Opatz, I. L. A transient developmental increase in prefrontal activity alters network maturation and causes cognitive dysfunction in adult mice. *Neuron* **109**, 1350-1364.e1356, doi:10.1016/j.neuron.2021.02.011 (2021).

9 Larsen, B. & Luna, B. Adolescence as a neurobiological critical period for the development of higher-order cognition. *Neuroscience & Biobehavioral Reviews* **94**, 179-195, doi:https://doi.org/10.1016/j.neubiorev.2018.09.005 (2018).

10 Bicks, L. K. *et al.* Prefrontal parvalbumin interneurons require juvenile social experience to establish adult social behavior. *Nat Commun* **11**, 1003, doi:10.1038/s41467-020-14740-z (2020).

11 Weinberger, D. R. & Berman, K. F. Prefrontal function in schizophrenia: confounds and controversies. *Philos Trans R Soc Lond B Biol Sci* **351**, 1495-1503, doi:10.1098/rstb.1996.0135 (1996).

12 Sakurai, T. & Gamo, N. J. Cognitive functions associated with developing prefrontal cortex during adolescence and developmental neuropsychiatric disorders. *Neurobiology of Disease* **131**, 104322, doi:https://doi.org/10.1016/j.nbd.2018.11.007 (2019).

13 Insel, T. R. Rethinking schizophrenia. *Nature* **468**, 187-193, doi:10.1038/nature09552 (2010).

14 Feinberg, I. & Campbell, I. G. Sleep EEG changes during adolescence: an index of a fundamental brain reorganization. *Brain Cogn* **72**, 56-65, doi:10.1016/j.bandc.2009.09.008 (2010).

15 Marenco, S. *et al.* Investigation of anatomical thalamo-cortical connectivity and FMRI activation in schizophrenia. *Neuropsychopharmacology : official publication of the American College of Neuropsychopharmacology* **37**, 499-507, doi:10.1038/npp.2011.215 (2012).

16 Kubota, M. *et al.* Thalamocortical disconnection in the orbitofrontal region associated with cortical thinning in schizophrenia. *JAMA Psychiatry* **70**, 12-21, doi:10.1001/archgenpsychiatry.2012.1023 (2013).

17 Katz, M. *et al.* Correlational patterns of cerebral glucose metabolism in never-medicated schizophrenics. *Neuropsychobiology* **33**, 1-11 (1996).

18 Woodward, N. D., Karbasforoushan, H. & Heckers, S. Thalamocortical dysconnectivity in schizophrenia. *Am J Psychiatry* **169**, 1092-1099, doi:10.1176/appi.ajp.2012.12010056 (2012).

19 Mitelman, S. A., Byne, W., Kemether, E. M., Hazlett, E. A. & Buchsbaum, M. S. Metabolic disconnection between the mediodorsal nucleus of the thalamus and cortical Brodmann's areas of the

left hemisphere in schizophrenia. *The American journal of psychiatry* **162**, 1733-1735, doi:162/9/1733 [pii]

10.1176/appi.ajp.162.9.1733 (2005).

20 Pinault, D. & Deschenes, M. Projection and innervation patterns of individual thalamic reticular axons in the thalamus of the adult rat: a three-dimensional, graphic, and morphometric analysis. *J Comp Neurol* **391**, 180-203 (1998).

21 Giraldo-Chica, M., Rogers, B. P., Damon, S. M., Landman, B. A. & Woodward, N. D. Prefrontal-Thalamic Anatomical Connectivity and Executive Cognitive Function in Schizophrenia. *Biol Psychiatry*, doi:10.1016/j.biopsych.2017.09.022 (2017).

22 Woodward, N. D. & Heckers, S. Mapping Thalamocortical Functional Connectivity in Chronic and Early Stages of Psychotic Disorders. *Biological psychiatry* **79**, 1016-1025, doi:10.1016/j.biopsych.2015.06.026 (2016).

23 Anticevic, A. *et al.* Association of Thalamic Dysconnectivity and Conversion to Psychosis in Youth and Young Adults at Elevated Clinical Risk. *JAMA Psychiatry* **72**, 882-891, doi:10.1001/jamapsychiatry.2015.0566 (2015).

24 Anticevic, A. *et al.* Characterizing thalamo-cortical disturbances in schizophrenia and bipolar illness. *Cereb Cortex* **24**, 3116-3130, doi:10.1093/cercor/bht165 (2014).

25 Cho, K. I. *et al.* Altered Thalamo-Cortical White Matter Connectivity: Probabilistic Tractography Study in Clinical-High Risk for Psychosis and First-Episode Psychosis. *Schizophrenia bulletin* **42**, 723-731, doi:10.1093/schbul/sbv169 (2016).

26 Bolkan, S. S. *et al.* Thalamic projections sustain prefrontal activity during working memory maintenance. *Nat Neurosci* **20**, 987-996, doi:10.1038/nn.4568 (2017).

27 Parnaudeau, S., Bolkan, S. S. & Kellendonk, C. The Mediodorsal Thalamus: An Essential Partner of the Prefrontal Cortex for Cognition. *Biol Psychiatry* **83**, 648-656, doi:10.1016/j.biopsych.2017.11.008 (2018).

28 Rikhye, R. V., Gilra, A. & Halassa, M. M. Thalamic regulation of switching between cortical representations enables cognitive flexibility. *Nature neuroscience* **21**, 1753-1763, doi:10.1038/s41593-018-0269-z (2018).

29 Rikhye, R. V., Wimmer, R. D. & Halassa, M. M. Toward an Integrative Theory of Thalamic Function. *Annual review of neuroscience* **41**, 163-183, doi:10.1146/annurev-neuro-080317-062144 (2018).

30 Schmitt, L. I. *et al.* Thalamic amplification of cortical connectivity sustains attentional control. *Nature* **545**, 219-223, doi:10.1038/nature22073 (2017).

31 Hsiao, K. *et al.* A Thalamic Orphan Receptor Drives Variability in Short-Term Memory. *Cell* **183**, 522-536.e519, doi:https://doi.org/10.1016/j.cell.2020.09.011 (2020).

32 Saalmann, Y. B. Intralaminar and medial thalamic influence on cortical synchrony, information transmission and cognition. *Front Syst Neurosci* **8**, 83, doi:10.3389/fnsys.2014.00083 (2014).

33 Parnaudeau, S. *et al.* Inhibition of mediodorsal thalamus disrupts thalamofrontal connectivity and cognition. *Neuron* **77**, 1151-1162, doi:10.1016/j.neuron.2013.01.038 (2013).

34 Benoit, L. J. *et al.* Medial prefrontal lesions impair performance in an operant delayed nonmatch to sample working memory task. *Behav Neurosci*, doi:10.1037/bne0000357 (2020).

35 Bissonette, G. B. *et al.* Double dissociation of the effects of medial and orbital prefrontal cortical lesions on attentional and affective shifts in mice. *J Neurosci* **28**, 11124-11130, doi:10.1523/JNEUROSCI.2820-08.2008 (2008).

36 Birrell, J. M. & Brown, V. J. Medial frontal cortex mediates perceptual attentional set shifting in the rat. *J Neurosci* **20**, 4320-4324 (2000).

37 Guirado, R., Umemori, J., Sipila, P. & Castren, E. Evidence for Competition for Target Innervation in the Medial Prefrontal Cortex. *Cereb Cortex* **26**, 1287-1294, doi:10.1093/cercor/bhv280 (2016).

38 Goodwill, H. L. *et al.* Early Life Stress Drives Sex-Selective Impairment in Reversal Learning by Affecting Parvalbumin Interneurons in Orbitofrontal Cortex of Mice. *Cell Rep* **25**, 2299-2307 e2294, doi:10.1016/j.celrep.2018.11.010 (2018).

39 Canetta, S. *et al.* Maternal immune activation leads to selective functional deficits in offspring parvalbumin interneurons. *Mol Psychiatry* **21**, 956-968, doi:10.1038/mp.2015.222 (2016).

40 Cho, K. K. *et al.* Gamma rhythms link prefrontal interneuron dysfunction with cognitive inflexibility in Dlx5/6(+/-) mice. *Neuron* **85**, 1332-1343, doi:10.1016/j.neuron.2015.02.019 (2015).

41 Cho, K. K. A. *et al.* Cross-hemispheric gamma synchrony between prefrontal parvalbumin interneurons supports behavioral adaptation during rule shift learning. *Nature neuroscience* **23**, 892-902, doi:10.1038/s41593-020-0647-1 (2020).

42 Mukherjee, A., Carvalho, F., Eliez, S. & Caroni, P. Long-Lasting Rescue of Network and Cognitive Dysfunction in a Genetic Schizophrenia Model. *Cell* **178**, 1387-1402 e1314, doi:10.1016/j.cell.2019.07.023 (2019).

43 Yuste, R. From the neuron doctrine to neural networks. *Nature reviews. Neuroscience* **16**, 487-497, doi:10.1038/nrn3962 (2015).

44 Stefanini, F. *et al.* A Distributed Neural Code in the Dentate Gyrus and in CA1. *Neuron* **107**, 703-716 e704, doi:10.1016/j.neuron.2020.05.022 (2020).

45 Narayanan, N. S. & Laubach, M. Methods for studying functional interactions among neuronal populations. *Methods Mol Biol* **489**, 135-165, doi:10.1007/978-1-59745-543-5_7 (2009).

46 Bernardi, S. *et al.* The Geometry of Abstraction in the Hippocampus and Prefrontal Cortex. *Cell* **183**, 954-967 e921, doi:10.1016/j.cell.2020.09.031 (2020).

47 Bitzenhofer, S. H., Pöpplau, J. A., Chini, M., Marquardt, A. & Hanganu-Opatz, I. L. A transient developmental increase in prefrontal activity alters network maturation and causes cognitive dysfunction in adult mice. *Neuron*, doi:10.1016/j.neuron.2021.02.011 (2021).

48 Larsen, B. & Luna, B. Adolescence as a neurobiological critical period for the development of higher-order cognition. *Neurosci Biobehav Rev* **94**, 179-195, doi:10.1016/j.neubiorev.2018.09.005 (2018).

49 Hill, R. A., Wu, Y. W., Kwek, P. & van den Buuse, M. Modulatory effects of sex steroid hormones on brain-derived neurotrophic factor-tyrosine kinase B expression during adolescent development in C57Bl/6 mice. *J Neuroendocrinol* **24**, 774-788, doi:10.1111/j.1365-2826.2012.02277.x (2012).

50 Flores-Barrera, E. *et al.* Late adolescent expression of GluN2B transmission in the prefrontal cortex is input-specific and requires postsynaptic protein kinase A and D1 dopamine receptor signaling. *Biol Psychiatry* **75**, 508-516, doi:10.1016/j.biopsych.2013.07.033 (2014).

51 Baker, K. D., Gray, A. R. & Richardson, R. The development of perineuronal nets around parvalbumin gabaergic neurons in the medial prefrontal cortex and basolateral amygdala of rats. *Behav Neurosci* **131**, 289-303, doi:10.1037/bne0000203 (2017).

52 Fagiolini, M. & Hensch, T. K. Inhibitory threshold for critical-period activation in primary visual cortex. *Nature* **404**, 183-186, doi:10.1038/35004582 (2000).

53 Morgunova, A. & Flores, C. MicroRNA regulation of prefrontal cortex development and psychiatric risk in adolescence. *Semin Cell Dev Biol*, doi:10.1016/j.semcdb.2021.04.011 (2021).

54 Paus, T., Keshavan, M. & Giedd, J. N. Why do many psychiatric disorders emerge during adolescence? *Nature reviews. Neuroscience* **9**, 947-957, doi:10.1038/nrn2513 (2008).

55 Caballero, A., Flores-Barrera, E., Cass, D. K. & Tseng, K. Y. Differential regulation of parvalbumin and calretinin interneurons in the prefrontal cortex during adolescence. *Brain Struct Funct* **219**, 395-406, doi:10.1007/s00429-013-0508-8 (2014).

56 Chini, M. & Hanganu-Opatz, I. L. Prefrontal Cortex Development in Health and Disease: Lessons from Rodents and Humans. *Trends Neurosci* **44**, 227-240, doi:10.1016/j.tins.2020.10.017 (2021).

57 Konstantoudaki, X. *et al.* Prefrontal cortical-specific differences in behavior and synaptic plasticity between adolescent and adult mice. *J Neurophysiol* **119**, 822-833, doi:10.1152/jn.00189.2017 (2018).

58 Caballero, A., Flores-Barrera, E., Thomases, D. R. & Tseng, K. Y. Downregulation of parvalbumin expression in the prefrontal cortex during adolescence causes enduring prefrontal disinhibition in adulthood. *Neuropsychopharmacology* **45**, 1527-1535, doi:10.1038/s41386-020-0709-9 (2020).

59 Miyamae, T., Chen, K., Lewis, D. A. & Gonzalez-Burgos, G. Distinct Physiological Maturation of Parvalbumin-Positive Neuron Subtypes in Mouse Prefrontal Cortex. *J Neurosci* **37**, 4883-4902, doi:10.1523/JNEUROSCI.3325-16.2017 (2017).

60 Yang, J. M., Zhang, J., Yu, Y. Q., Duan, S. & Li, X. M. Postnatal development of 2 microcircuits involving fast-spiking interneurons in the mouse prefrontal cortex. *Cereb Cortex* **24**, 98-109, doi:10.1093/cercor/bhs291 (2014).

61 Bitzenhofer, S. H., Popplau, J. A. & Hanganu-Opatz, I. Gamma activity accelerates during prefrontal development. *eLife* **9**, doi:10.7554/eLife.56795 (2020).

62 Delevich, K., Klinger, M., Okada, N. J. & Wilbrecht, L. Coming of age in the frontal cortex: The role of puberty in cortical maturation. *Seminars in Cell & Developmental Biology*, doi:https://doi.org/10.1016/j.semcdb.2021.04.021 (2021).

63 Zuo, Y., Lin, A., Chang, P. & Gan, W.-B. Development of Long-Term Dendritic Spine Stability in Diverse Regions of Cerebral Cortex. *Neuron* **46**, 181-189, doi:https://doi.org/10.1016/j.neuron.2005.04.001 (2005).

64 Pattwell, S. S. *et al.* Dynamic changes in neural circuitry during adolescence are associated with persistent attenuation of fear memories. *Nat Commun* **7**, 11475, doi:10.1038/ncomms11475 (2016).

65 Marmolejo, N., Paez, J., Levitt, J. B. & Jones, L. B. Early postnatal lesion of the medial dorsal nucleus leads to loss of dendrites and spines in adult prefrontal cortex. *Dev Neurosci* **34**, 463-476, doi:10.1159/000343911 (2012).

66 Van Eden, C. G. & Uylings, H. B. Postnatal volumetric development of the prefrontal cortex in the rat. *J Comp Neurol* **241**, 268-274, doi:10.1002/cne.902410303 (1985).

67 Ferguson, B. R. & Gao, W. J. Development of thalamocortical connections between the mediodorsal thalamus and the prefrontal cortex and its implication in cognition. *Frontiers in human neuroscience* **8**, 1027, doi:10.3389/fnhum.2014.01027 (2014).

68 Uhlhaas, P. J. & Singer, W. The development of neural synchrony and large-scale cortical networks during adolescence: relevance for the pathophysiology of schizophrenia and neurodevelopmental hypothesis. *Schizophrenia bulletin* **37**, 514-523, doi:10.1093/schbul/sbr034 (2011).

69 Wen, W. & Turrigiano, G. G. Developmental Regulation of Homeostatic Plasticity in Mouse Primary Visual Cortex. *bioRxiv*, 2021.2006.2011.448148, doi:10.1101/2021.06.11.448148 (2021).

70 Wu, C. H., Ramos, R., Katz, D. B. & Turrigiano, G. G. Homeostatic synaptic scaling establishes the specificity of an associative memory. *Curr Biol* **31**, 2274-2285 e2275, doi:10.1016/j.cub.2021.03.024 (2021).

71 Rios, O. & Villalobos, J. Postnatal development of the afferent projections from the dorsomedial thalamic nucleus to the frontal cortex in mice. *Brain Res Dev Brain Res* **150**, 47-50, doi:10.1016/j.devbrainres.2004.02.005 (2004).

72 Guo, Z. V. *et al.* Maintenance of persistent activity in a frontal thalamocortical loop. *Nature* **545**, 181-186, doi:10.1038/nature22324 (2017).

73 Kamigaki, T. & Dan, Y. Delay activity of specific prefrontal interneuron subtypes modulates memory-guided behavior. *Nature neuroscience* **20**, 854-863, doi:10.1038/nn.4554 (2017).

74 Spellman, T., Svei, M., Kaminsky, J., Manzano-Nieves, G. & Liston, C. Prefrontal deep projection neurons enable cognitive flexibility via persistent feedback monitoring. *Cell* **184**, 2750-2766 e2717, doi:10.1016/j.cell.2021.03.047 (2021).

75 Canetta, S. *et al.* Maternal immune activation does not alter the number of perisomatic parvalbumin-positive boutons in the offspring prefrontal cortex. *Mol Psychiatry* **21**, 857, doi:10.1038/mp.2016.92 (2016).

76 Vinck, M., van Wingerden, M., Womelsdorf, T., Fries, P. & Pennartz, C. M. The pairwise phase consistency: a bias-free measure of rhythmic neuronal synchronization. *Neuroimage* **51**, 112-122, doi:10.1016/j.neuroimage.2010.01.073 (2010).

Figures

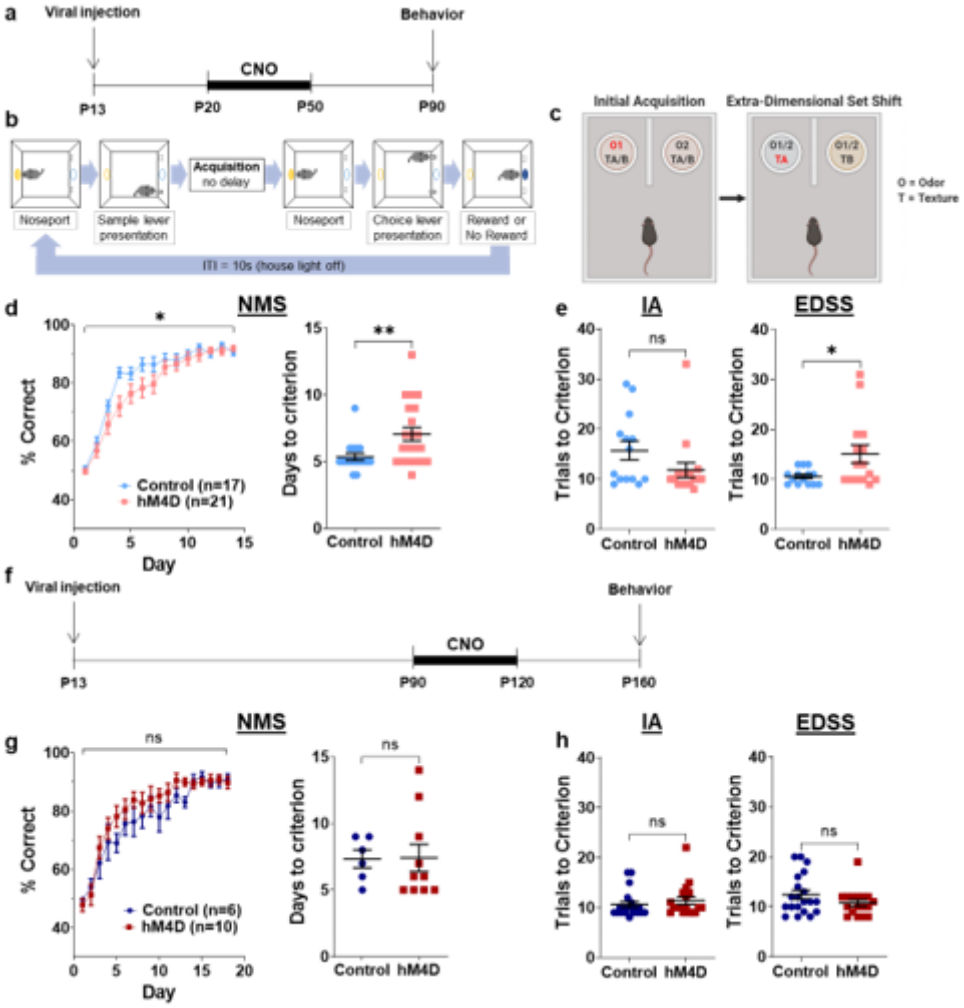

Figure 1

Adolescent thalamic inhibition leads to persistent behavioral impairments in adulthood, while adult thalamic inhibition does not. Schematics of (a) the Non-Match to Sample (NMS) task and (b) the attentional set-shifting task (ASST). (c) Adolescent experimental timeline. CNO was administered from P20-50 to mice expressing hM4D or GFP in the thalamus, and behavior was conducted 40 days later, at P90. (d) Adolescent-inhibited hM4D animals take significantly longer to acquire the NMS task (left), taking significantly more days to reach criterion (right). Control: n=17; hM4D: n=21; learning curve: 2-way repeated measures (rm) ANOVA, effect of time $F(4.201,151.2)=102.0$, $p<0.0001$, effect of group $F(1,36)=3.143$, $p=0.0847$, effect of group x time $F(13,468)=2.088$, *$p=0.0137$; days to criterion (3 consecutive days above 70%): Control: (mean ± standard error of the mean, SEM) 5.35±0.27 days, hM4D: 7.05±0.51 days; unpaired t-test: $t=2.746$, $df=36$, **$p=0.0094$. (e) Adolescent-inhibited hM4D animals are no different than controls in the initial acquisition (IA) of the ASST (left, n=14 Control animals, n=16 hM4D animals; Control: 15.71±1.88 days, hM4D: 11.81±1.50 days; unpaired t-test, $t=1.639$, $df=28$, $p=0.1125$) but take significantly more trials in the extra-dimensional set shift (EDSS) than controls (right, n=14 Control animals, n=15 hM4D animals; Control: 10.57±0.42 days, hM4D: 15.07±1.79 days; unpaired t-test, $t=2.372$, $df=27$, *$p=0.0251$). (f) Adult experimental timeline, with CNO administered P90-120 and testing at P160. There were no differences in either (g) the acquisition of the NMS task (n=6 Control

animals, n=10 hM4D animals; learning curve: 2-way rmANOVA, effect of time F(5.501,77.01)=40.21, p<0.0001, effect of group F(1,14)=1.462, p=0.2467, effect of group x time F(17,238)=0.8680, p=0.6126; days to criterion: Control: 7.33±0.67 days, hM4D: 7.40±1.02 days; unpaired t-test, t=0.04654, df=14, p=0.9635) or (h) the IA (Control: n=20; hM4D: n=18; Control: 10.60±0.59 days, hM4D: 11.39±0.76 days; unpaired t-test, t=0.8260, df=36, p=0.4142) and EDSS (Control: 12.40±0.89 days, hM4D: 10.76±0.64 days; unpaired t-test, t=1.442, df=35, p=0.1583) portions of the ASST between adult-inhibited hM4D animals and controls. Learning curves depict mean performance ± SEM for each day. For other plots, dots represent individual animals; lines represent mean ± SEM. *p<0.05, **p<0.01

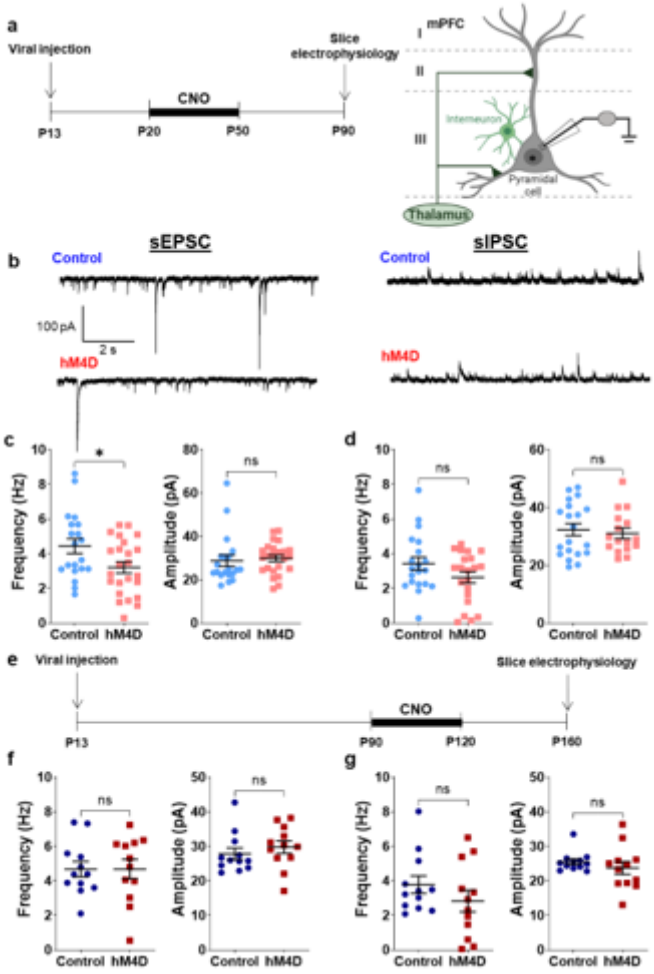

Figure 2

Adolescent thalamic inhibition leads to a persistent decrease in mPFC pyramidal excitation in adulthood, while adult thalamic inhibition does not. (a) Adolescent experimental timeline and schematic. Whole cell patch clamp recordings were made from pyramidal cells in layer II/III of the mPFC from hM4D and control mice. These pyramidal cells receive excitatory inputs from the midline thalamus as well as inhibitory inputs from local interneurons. (b) Representative traces showing spontaneous excitatory post-synaptic currents (sEPSCs, left) and spontaneous inhibitory post-synaptic currents (sIPSCs, right). (c) sEPSC frequency is significantly reduced following adolescent thalamic inhibition relative to control mice, but sEPSC amplitude is unchanged. Control: n=20 cells, 5 animals; hM4D: n=24 cells, 7 animals;

frequency: Control: 4.438±0.429 Hz, hM4D: 3.202±0.325 Hz; unpaired t-test, t=2.337, df=42, *p=0.0243; amplitude: Control: 28.71±2.57 pA, hM4D: 29.82±1.47 pA; unpaired student's t-test, t=0.3881, df=42, p=0.6999. (d) sIPSC frequency and amplitude are also unchanged. Control: n=20 cells, 5 animals; hM4D: n=21 cells, 7 animals; frequency: Control: 3.421±0.376 Hz, hM4D: 2.627±0.323 Hz; unpaired t-test, t=1.606, df=39, p=0.1163; amplitude: Control: 32.29±2.08 pA, hM4D: 31.03±1.84 pA; unpaired t-test, t=0.4450, df=34, p=0.6592. (e) Adult experimental timeline. (f) sEPSC and (g) sIPSC frequency and amplitude are unchanged following adult thalamic inhibition. Control: n=12 cells, 3 animals; hM4D: n=12 cells, 3 animals; sEPSC: n=12 Control cells, n=12 hM4D cells; frequency: Control: 4.674±0.448 Hz, hM4D: 4.675±0.561 Hz; unpaired t-test, t=0.001936, df=22, p=0.9985; amplitude: Control: 27.78±1.68 pA, hM4D: 29.75±1.78 pA; unpaired t-test, t=0.8048, df=22, p=0.4296; sIPSC: n=12 Control cells, n=12 hM4D cells; frequency: Control: 3.775±0.506 Hz, hM4D: 2.825±0.625 Hz; unpaired t-test, t=1.181, df=22, p=0.2501; amplitude: Control: 25.49±0.82 pA, hM4D: 23.69±1.82 pA; unpaired t-test, t=0.9030, df=22, p=0.3763. Dots represent individual animals; lines represent mean ± SEM. *p<0.05

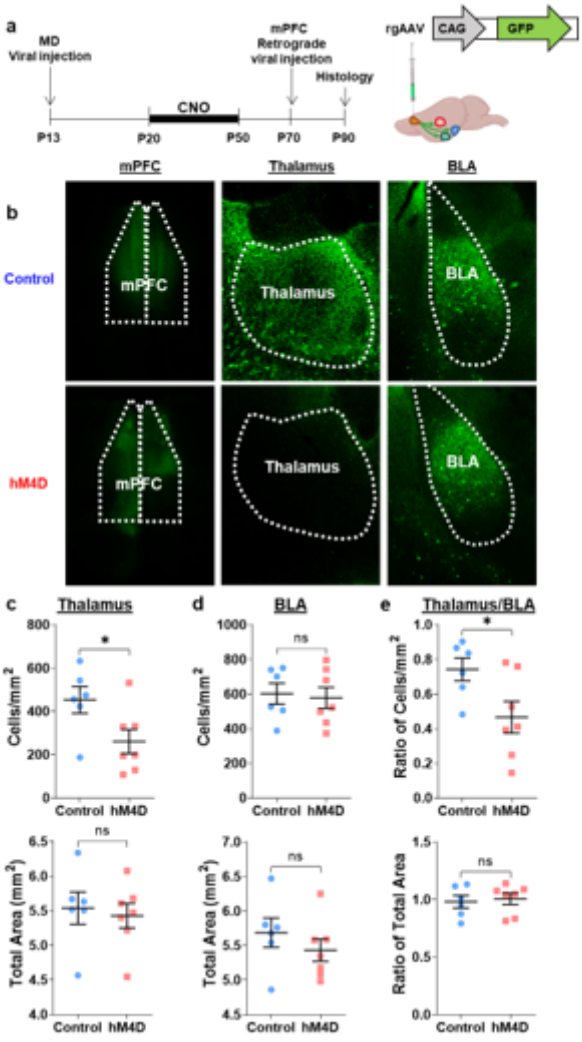

Figure 3

Adolescent thalamic inhibition leads to persistent anatomical changes in adulthood, reducing the number of projections to the mPFC from the thalamus, but not from the BLA. (a) Experimental timeline and

schematic. At P70, a retrograde tracer, GFP, was injected into the mPFC, before perfusion 3 weeks later. (b) Representative confocal images illustrating GFP staining in the mPFC (left), thalamus (middle), and basolateral amygdala (BLA, right) in control (top) and hM4D (bottom) animals. Outlines were determined using DAPI staining. (c) Stereology was conducted using DAPI staining for outlines of regions and GFP staining for cell counting. Quantification of GFP-positive cell density showed a significant decrease in thalamo-mPFC projecting cells in adolescent-inhibited hM4D animals compared to controls (top, Control: 453.2±61.3 cells/mm2, hM4D: 260.3±56.1 cells/mm2; unpaired t-test, t=2.326, df=11, *p=0.0401). Stereological estimates showed no difference in overall thalamic area (bottom, Control: 5.539±0.232 mm2, hM4D: 5.429±0.178 mm2; unpaired t-test, t=0.3834, df=11, p=0.7087). (d) Stereology in the BLA showed no differences in either GFP-positive cell density (top, Control: 602.4±61.1 cells/mm2, hM4D: 578.5±61.0 cells/mm2; unpaired t-test, t=0.2749, df=11, p=0.7885) or BLA area (bottom, Control: 5.687±0.211 mm2, hM4D: 5.432±0.163 mm2; unpaired t-test, t=0.9713, df=11, p=0.3523). (e) The ratio of thalamic to BLA projection cell densities showed a significant reduction in adolescent-inhibited hM4D animals compared to controls (top, Control: 0.742±0.065, hM4D: 0.467±0.091; unpaired t-test, t=2.376, df=11, *p=0.0368) but no change in region area (bottom, Control: 0.981±0.055, hM4D: 1.006±0.049; unpaired t-test, t=0.3471, df=11, p=0.7351). Control: n=6, hM4D: n=7. Dots represent individual animals; lines represent mean ± SEM. *p<0.05

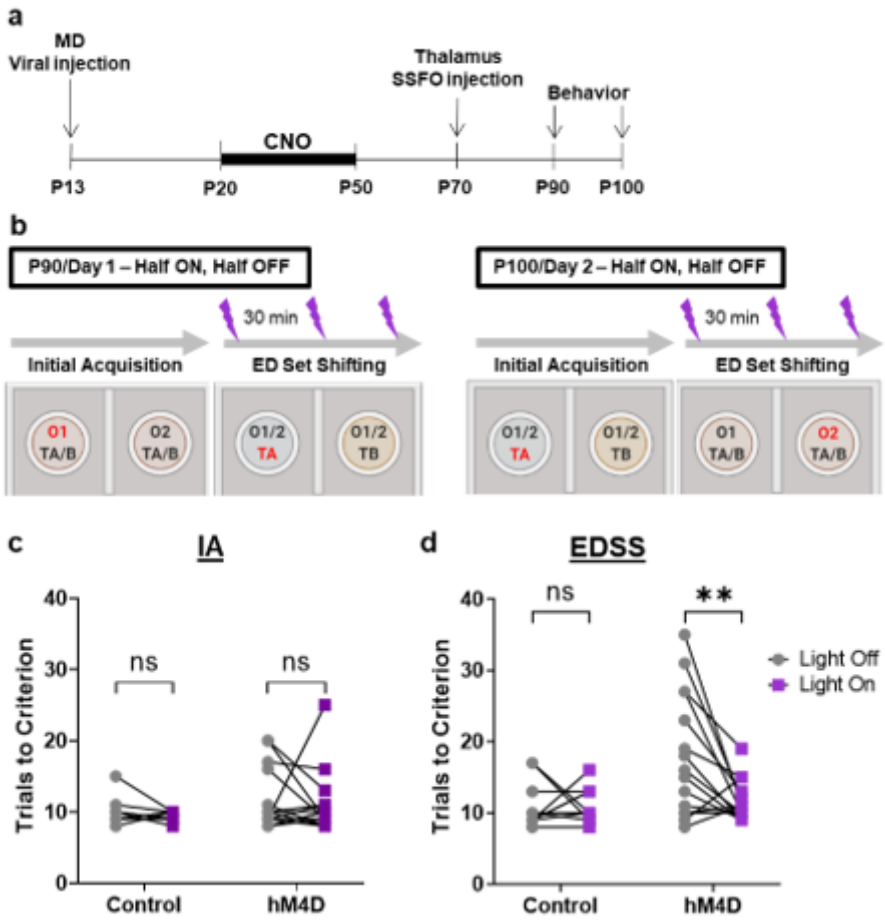

Figure 4

Acute thalamic activity enhancement rescues the ASST behavioral deficit following adolescent thalamic inhibition. (a) Experimental timeline. At P70, a stabilized step-function opsin (SSFO) was injected into the thalamus along with optrodes. Behavior was done at P90 and P100. (b) Schematic for behavior. For the light ON animals, the SSFO was stimulated before the EDSS and again every 30 min during the inter-trial interval (ITI) until completion of the task. Animals were randomly assigned to two groups: (1) light ON (SSFO activation) on Day 1 at P90 and light OFF on Day 2 at P100; (2) light OFF on Day 1 at P90 and light ON on Day 2 at P100. (c) There is no significant difference in IA performance between the control or hM4D light OFF groups. Further, all groups showed equivalent trials to criterion during the IA (2-way rmANOVA; effect of group $F(1,23)=2.407$, $p=0.1344$, effect of light $F(1,23)=0.3319$, $p=0.5702$, effect of virus x light $F(1,23)=0.001148$, $p=0.9733$; Holm-Sidak post-hoc: Control Light OFF vs. ON $p=0.8925$, hM4D Light OFF vs. ON $p=0.8925$). (d) hM4D light OFF animals take significantly more trials to reach criterion during EDSS compared with control light OFF animals. Acute SSFO stimulation (light ON) during the EDSS rescued the behavior in the adolescent-inhibited hM4D animals but had no effect on control animals (2-way rmANOVA; effect of group $F(1,23)=5.407$, $p=0.0292$, effect of light $F(1,23)=5.002$, $p=0.0353$, effect of virus x light $F(1,23)=5.002$, $p=0.0353$; Holm-Sidak post-hoc: Control Light OFF vs. ON $p>0.9999$, hM4D Light OFF vs. ON $^{**}p=0.0035$). Dots represent individual animals, lines connecting performance with light OFF and light ON. Control: n=10; hM4D: n=15. $^{**}p<0.01$

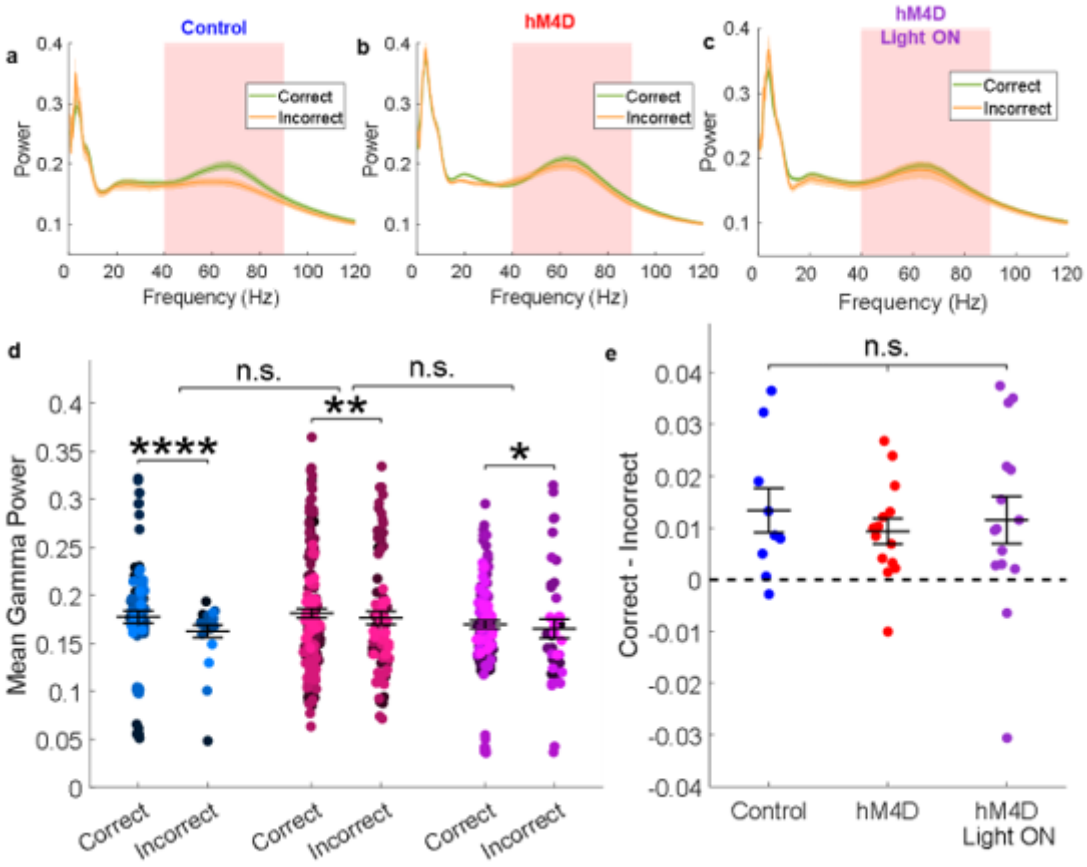

Figure 5

Adolescent thalamic inhibition does not significantly alter the mPFC gamma signature during the EDSS, and it is not changed by acute thalamic activation. (a) Control animal mPFC normalized power (artificial

units, A.U.) as a function of frequency during the 6 seconds preceding the decision point during the EDSS during correct trials (green), and incorrect trials (orange). Red shading indicates 40-90 Hz (gamma). Lines and shading indicate mean ± SEM. (b) As in (a), but for adolescent-inhibited hM4D animals. (c) As in (a), but for adolescent-inhibited hM4D animals that have acute SSFO activation during EDSS. (d) Mean gamma power (40-90 Hz) is significantly increased in correct vs incorrect trials for all three groups, and this pattern is not significantly different across groups. Control: left, blue; hM4D: center, pink; hM4D Light ON: right, purple. Lines and error represent mean ± SEM. Dots represent individual trials for each animal (colors of the dots). Control: n=9 animals, 88 correct trials, 23 incorrect trials, Correct: 0.1774±0.0064; Incorrect: 0.1625±0.0066; linear mixed effects model: fixed effect (Trial Type), ****p=5.1208e-05; hM4D: n=14 animals, 177 correct trials, 89 incorrect trials, Correct: 0.1813±0.0048; Incorrect: 0.1765±0.0068; linear mixed effects model: fixed effect (Trial Type), **p=0.0014916; hM4D Light ON: n=15 animals, 137 correct trials, 41 incorrect trials, Correct: 0.1697±0.0043; Incorrect: 0.1652±0.0099; linear mixed effects model: fixed effect (Trial Type), *p=0.015341. Linear hypothesis F-test to compare differences: Control vs. hM4D: p=0.3092; hM4D vs. hM4D Light ON: p=0.7607. (e) Mean difference in gamma power between correct and incorrect trials by animal shows no differences across groups, all groups having an increased gamma power for correct over incorrect trials. Control: n=9, 0.0134±0.0043; hM4D: n=14, 0.0093±0.0025; hM4D Light ON: n=15, 0.0115±0.0045; 1-way ANOVA, F(2,35)=0.2329, p=0.7935. Lines and error represent mean ± SEM. Dots represent individual animal mean difference. *p<0.05, **p<0.01, ****p<0.0001

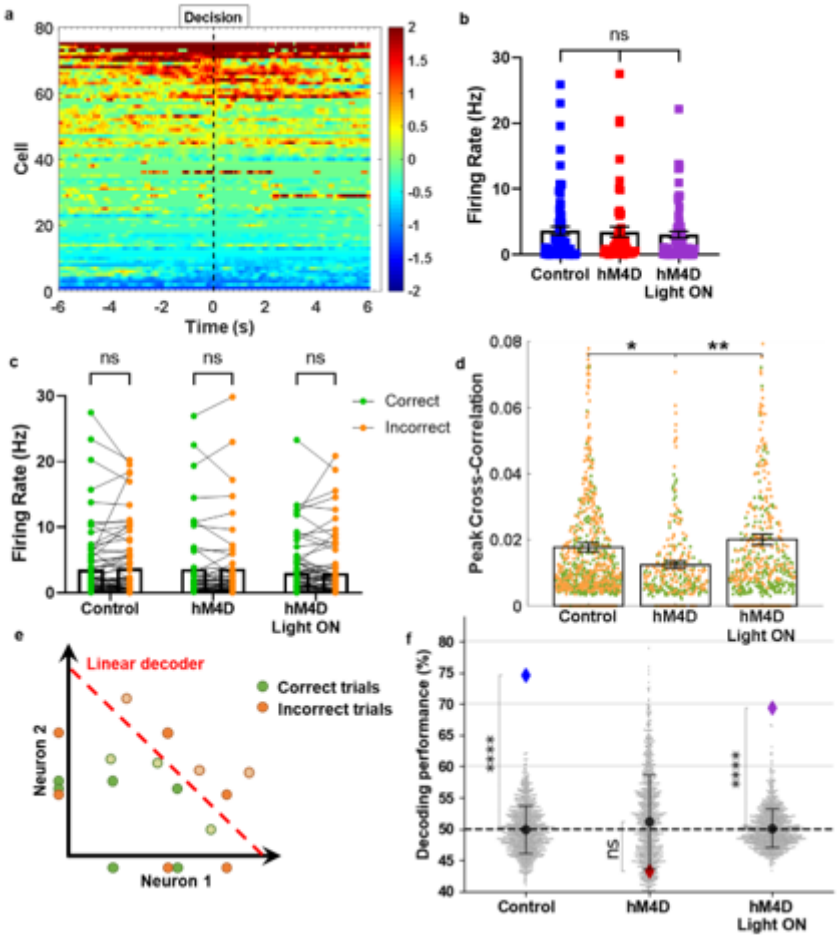

Figure 6

Adolescent thalamic inhibition leads to loss of mPFC cellular encoding of ASST trial outcome. (a) Control cell mean firing rate (FR) during EDSS, z-scored, normalized to the ITI. Time in s represents time before and after the decision point (dashed black line). Color scale represents z-score for each time bin. (b) FR during the trial across the different experimental conditions showed no changes in population activity. Control: n=8 animals, 75 cells; hM4D: n=12 animals, 55 cells; hM4D Light ON: n=13 animals, 71 cells, Control: 3.650±0.639 Hz; hM4D: 3.487±0.777 Hz; hM4D Light ON: 3.058±0.516 Hz; 1-way ANOVA, $F(2,194)=0.2493$, $p=0.7796$. Dots represent individual cells; lines represent mean ± SEM. (c) FR during correct rule and incorrect rule trials for cells from control animals (left), adolescent-inhibited hM4D animals (center), and thalamic-activated hM4D animals (right) show no differences in FR for different trial types. Dots represent individual cells, lines connecting FR for correct and incorrect trials. Control: FR during Correct: 3.570±0.647 Hz, Incorrect: 3.744±0.630 Hz; paired t-test: $t=0.6546$, $df=71$, $p=0.5148$; hM4D: Correct: 3.607±0.859 Hz, Incorrect: 3.676±0.873 Hz; paired t-test: $t=0.3174$, $df=48$, $p=0.7523$; hM4D Light ON: Correct: 3.058±0.519 Hz, Incorrect: 3.023±0.550 Hz; paired t-test: $t=0.1539$, $df=70$, $p=0.8781$. (d) Peak cross-correlation values for each pair of cells within an animal during correct (green) and incorrect (orange) trials across experimental conditions shows decreased cross-correlations in adolescent-inhibited hM4D animals compared to both control and rescued thalamic activation animals. Bars with error represent mean ± SEM. Individual dots represent cell pair correlations for each trial outcome type. This graph has been truncated along the y-axis to better demonstrate the mean and standard deviation. The complete distribution, along with the firing patterns of the truncated cells, in supplemental figure 7. Control: n=6 animals, 73 cells, 507 cell pairs; hM4D: n=9 animals, 52 cells, 181 cell pairs; hM4D Light ON: n=11 animals, 69 cells, 327 cell pairs; Control: 0.0177±0.0430; hM4D: 0.0124 ±0.0212; hM4D Light ON: 0.0201±0.0414; linear mixed effects model, fixed effect of group: Control vs. hM4D: *p=0.041622; hM4D vs. hM4D Light ON: **p=0.0090838. (e) Schematic of the linear decoder. For a hypothetical pair of neurons, neither cell's firing rate alone shows a strong difference between correct and incorrect trial firing (dots along the x and y axes). However, when plotted together, it is possible to train a linear decoder (red dashed line) to discriminate between trial outcomes. With this training, we can then test the decoder on additional trials (lightly shaded circles). In this example, the linear decoder performs at 100%. (f) Decoding trial outcome using FR during the EDSS. Decoder performance is significantly above chance for control animals, at chance for hM4D animals, and rescued by acute thalamic activation. Actual decoder performance in colored diamonds (Control: blue; hM4D: red; hM4D Light ON: purple). Shuffled trial outcomes show chance decoder performance, mean ± standard deviation (black circles and error bars) and individual shuffles (grey circles). Control: n=4 animals, 60 cells, 1000 shuffles; hM4D: n=7 animals, 45 cells, 1000 shuffles; hM4D Light ON: n=9 animals, 61 cells, 1000 shuffles; Control: 74.71%, shuffled performance: 49.95±3.75%, ****p=3.9604e-11; hM4D: 43.25%, shuffled performance: 51.13±7.49%, p=0.2926; hM4D Light ON: 69.41%, shuffled performance: 50.15±3.08%, ****p=3.9472e-10. *p<0.05, **p<0.01, ****p<0.0001

Supplementary Files

This is a list of supplementary files associated with this preprint. Click to download.

- SupplementalFigures.docx